Magnetic compensation and stabilization for the BaF eEDM search experiment

Bachelor Thesis

B. Cornelis Zandt
S2482959
22-12-2017

Prof. Dr. K.H.K.J. Jungmann
Dr. L. Willman

Rijksuniversiteit Groningen – VSI/FIS

Content

1. Introduction

In physics the world is described using various models and laws. After centuries of research multiple different models were accomplished, from basic mechanical models to the laws of Maxwell for electromagnetism. From the discovery of the electron by J.J. Thompson in 1897 [1] on, more and more particles were discovered. These particles were seen as fundamental building blocks of nature. In combination with discoveries on quantum physics and relativity, fundamental forces were ascribed to different particles in the first part of the 20th century. These combined into Quantum Electrodynamics described first by Feynman [2] to account for electromagnetic interactions with an exchange of a (virtual) photon [3]. With the discovery of the neutrino the first proposal by Fermi describing a then new interaction [4] was confirmed, and later with the discovery of the muon and a second neutrino this was unified to what is now sometimes called Quantum Flavourdynamics. It was Glashow in 1961 who first started to combine these two models [5] in the electroweak theory, laying the basis for what we now call the Standard Model in physics.

The discovery of the first three quarks shed a light on yet another force. Until the 70's it was still a mystery how the nuclei of atoms were hold together. But with the discovery of the quarks [6], it became clear that the protons and neutrons in the nuclei were not fundamental particles [7]. The nuclear interaction between these two was merely a side effect of these fundamental particles and the third fundamental force, the strong force, together with the concept of color sourcing this phenomenon, as explained by Quantum Chromodynamics. [8]

As the first two models were combined, the latter was added and the Standard Model of physics was born. This model is believed to be self-consistent and has been the basis of tremendous experimental successes. In particular, tests of the discrete symmetry breaking, charge conjugation C, parity P [9] and time-reversal T, has led to this model, and let to explore more and more phenomena. [10] One of these symmetry breakings in particular is the CP-violation [11], which arises from the CKM-matrix [12], the coupling matrix for quark transitions. With these transitions it is believed that virtual quarks are created, interact with electrons, and are annihilated, with the result that initial quarks have transited. Yet, for this interaction to be possible, through CP-odd operators, the existence of a finite electron electric dipole moment (eEDM) is needed [13].

Even though the Standard Model of physics has had such successes, it leaves some phenomena unexplained. Until now the theory of gravitation is not included in the standard model. Moreover, matter-antimatter asymmetry in the universe and the non-zero mass of the neutrino tells that fine-tuning of the Standard Model or theories beyond the Standard Model are needed. A model aiming to explain this gravitation problem is string theory [14], yet supersymmetry aims to extend the standard model to explain gravity [15]. Like these, there are more models and extensions of the Standard Model, to shape our understanding of how the world works.

To examine these models, precision tests in particle physics are needed. A kind of these precision tests is to examine the coupling constants of the interactions. As mentioned above, the eEDM relates to one of these constants, the Fermi coupling constant, defining the operator and thus interactions [13]. As the eEDM has some measurable value this could act as an excellent probe to include or exclude various models. The Standard Model in physics predicts a value for the eEDM

of the order of 10^{-38} e·cm [13], while the weak-scale supersymmetry yields an upper bound of 10^{-30} e·cm [16].

The current limit is set by the ACME collaboration in Stanford at $|d_e|<8.7\cdot10^{-29}$ e·cm using the polar molecule thorium monoxide [16]. However, new projects are aiming to improve this limit. The Fundamental Interaction and Symmetries group at the Van Swinderen Institue of Particle Physics in Groningen, together with the LaserLab in Amsterdam collaborate in doing so. The aim of the freshly started experiment is to measure or limit the eEDM with a sensitivity of $5\cdot10^{-30}$ e·cm using an intense cold beam of barium monofluoride molecules [17], extending the current minimum by an order of magnitude. For this improvement, a combination of state of the art technologies and methods must be used, and for the measurement of the eEDM an interaction zone is needed where the magnetic field is cancelled and controlled of order 10 pT.

In this thesis there will be elaborated on the essential parts of the theory relating to eEDM, how the eEDM can be measured with a $5\cdot10^{-30}$e·cm with using BaF, as the experiment in Groningen will strive for and the requirements to get this result. In particular the focus lies on the interaction zone, where a small magnetic field is needed. Several options for active and passive magnetic compensation will be described and in particular the active compensation of the magnetic field by an order of ten will be researched.

2. Theory

eEDM experiment in connection with particle physics

In this section is described what an EDM is and what its connection is to the violation of CP invariance. In classical electrodynamics, an electric dipole consists of two equal and opposite electric charges, $\pm q$, separated by a distance, **d**. The electric dipole moment in classical electrodynamics is therefore defined as [18]:

$$\boldsymbol{p} = q\mathbf{d} = \int \boldsymbol{r}'\rho(\boldsymbol{r}')\, d\tau', \tag{2.1}$$

where the last equation integrates over all charge in the system times there spacing r', and describes the general form. If this electric dipole enters a homogeneous electric field **E**, the dipole experiences a force. Although the net force on the system equals zero, the two different charges, experience an opposite force and are under a torque, $\boldsymbol{N}$, given by:

$$\boldsymbol{N} = \boldsymbol{p} \times \boldsymbol{E}. \tag{2.2}$$

In classical electrodynamics the electron is defined as one point charge. For a point charge an electric dipole moment is therefore impossible, since there are no two charges, or a charge difference, spaced from each other in a single point [18].

In quantum physics, magnetism is a completely quantum mechanical phenomenon [19].The electron has, due to its angular momentum, a magnetic moment, **μ**, given by:

$$\boldsymbol{\mu} = \frac{-q_e}{m}\, \mathbf{J} \text{ (electron spin)}, \tag{2.3}$$

where q_e is the electrons electric charge, m its mass and **J** its angular momentum. If this electron is placed inside a magnetic field, the electron will experience a torque. Because of the angular momentum of this electron, the magnetic moment in the magnetic field will not have the consequence of lining up, and they will start to precess around an axis in line with the magnetic field.

Following the same line of thought, if an electron has an intrinsic electric dipole moment, the electron will start to precess if placed inside an electric field. For the electric dipole moment the charge distribution is dependent on the angular momentum state of the particle [20],

$$d = \int \rho_{JJ} z \, \mathrm{d}\tau, \tag{2.4}$$

where it is not **p** denoting the electric dipole moment as in the classical view, but d is. Furthermore z is measured from the centre of mass of the particle, ρ_{JJ} is the charge density inside the particle whose angular momentum is **J** with quantum number J, whose orientation state is given by $m = J$ relative to the z axis. Note that because of the definition of J precessing around the z axis vector notation is supervacaneous.

Both effects together are depicted in figure 1, where the angular momentum is defined by the spin **S** of the electron, around the z-axis, also the E and B field point in the z-direction.

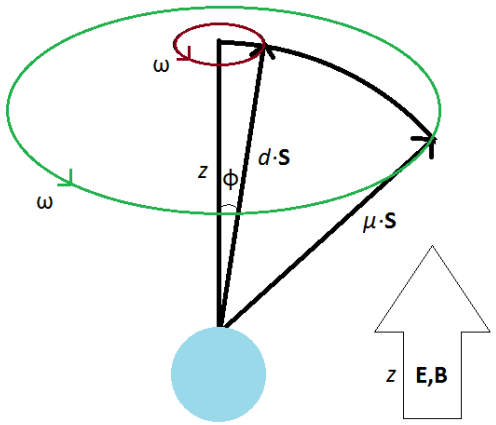

Figure 1: Schematic picture of the precession of the Spin of a non-relativistic electron placed in an electric and magnetic field.

Three fundamental symmetries in the laws of physics are charge conjugation C, parity P and time-reversal T. Where C is responsible for the change of particles to antiparticles, P for reflection of spatial coordinates and T of the reversal of time applicable to momentum. The CPT theorem states that the combination of the three are observed to be in symmetry for all physical phenomena [21].

In some weak interactions though, CP violating transitions have been observed [11]. These can be explained by the mixing of quarks, the mass eigenstates are not directly equal to the flavour eigenstates, giving rise to the decay of quarks. Kobayashi and Maskawa modelled these phenomena [12] and, elaborating on the work of Cabibbo, created the CKM mixing matrix,

$$\begin{pmatrix} c_1 & s_1c_3 & s_1s_3 \\ -s_1c_2 & c_1c_2c_3 - e^{i\delta}s_2s_3 & c_1c_2c_3 + e^{i\delta}s_2c_3 \\ s_1s_2 & -c_1s_2c_3 - e^{i\delta}c_2s_3 & -c_1s_2s_3 + e^{i\delta}c_2c_3 \end{pmatrix}, \tag{2.5}$$

where $c_i = cos(\theta_i)$, $s_i = sin(\theta_i)$ $(i=1,2,3)$ are the mixing angles and δ the complex phase, for which this violation occurs.

These CP-violating transitions occur via the continuous emittance and reabsorption of virtual particles of all types that exist in nature, like all charged particles do in quantum field theory. Yet, for these transitions to happen, the total system should be CPT invariant. It is the coupling of these charged particles to the virtual particles in loops in Feynman diagrams that lead to this invariance [22].

The Hamiltonian of the electron with an electron EDM itself violates two of these symmetries as well. The Hamiltonian of a particle in a magnetic and electric field, **B** and **E** respectively, is given by

$$H = -\mu\mathbf{B}\cdot\frac{\mathbf{S}}{S} - d\mathbf{E}\cdot\frac{\mathbf{S}}{S}, \tag{2.6}$$

where **S** is the particle spin, μ the magnetic moment and d the electric dipole moment. Applying the Parity operator to the Hamiltonian results in

$$H = -\mu\mathbf{B}\cdot\frac{\mathbf{S}}{S} + d\mathbf{E}\cdot\frac{\mathbf{S}}{S}, \tag{2.7}$$

since the **B·S** term is unaffected, because of its axial vector character and **E·S** picks up a minus sign. Therefore, since

$$PH = -\mu\mathbf{B}\cdot\frac{\mathbf{S}}{S} + d\mathbf{E}\cdot\frac{\mathbf{S}}{S} \neq \mp\left(-\mu\mathbf{B}\cdot\frac{\mathbf{S}}{S} - d\mathbf{E}\cdot\frac{\mathbf{S}}{S}\right) = \mp H, \tag{2.8}$$

The presence of a non-zero EDM violates parity conservation. Applying the time-reversal operator has the same effect, and thus time invariance is conflicted as well. However, if and only if both operators are applied simultaneously, a non-zero EDM could exist [13]. Yet, for this PT violation to hold one concludes that in the same process also CP must be violated for the CPT theorem to hold. Therefore the decay of quarks happens due to continuous creation of virtual quarks, which interact with electrons, and are annihilated, with the result that initial quarks have transited.

For different models these interactions appears as a different order effect. The interaction described above yields that the EDM appears at least as a second-order effect with a magnitude of at least G^2 [22], where G = 1.166 3787(6) × 10^{-5} GeV^{-2} [23] is the fermi weak interaction constant. This comes down for the eEDM to be larger than at the order of 10^{-35} e·cm [24]. Several predictions for the eEDM are given in figure 2. In the Standard Model, the eEDM only appears in a fourth loop level and is more supressed, it has a predicted value of $d_e < 10^{-38}$ e·cm [13].

Despite the very small value of d_e in the SM, it is widely expected that an observation of the eEDM is likely if the experimental sensitivity can be improved by a few orders of magnitude. The current limit of d_e is 8.7 × 10^{-29} e·cm established by the ACME collaboration in 2013, using the polar molecule ThO [16]. With the combination of new physics at the electroweak scale, plus extensions of the SM which describe asymmetric T interactions, new speculated values of d_e that are near the current experimental limit have risen. Experimental limits on the size of d_e already impose stringent constraints on supersymmetry and other physics beyond the SM [25].

At the VSI group in Groningen, together with the LaserLab in Amsterdam an experiment has started to improve this limit. In this experiment the value for d_e is aimed to be improved by an order of magnitude. In this experiment a combination of advanced atomic physics techniques are used, leading to a sensibility of 5 × 10^{-30} [17], which therefore has potential to make a major contribution to outstanding questions in both particle physics and cosmology. Figure 2 depicts the objective of this experiment, denoted by *this proposal*, together with values for d_e for various extensions of the Standard Model. The next section will elaborate more on this experiment.

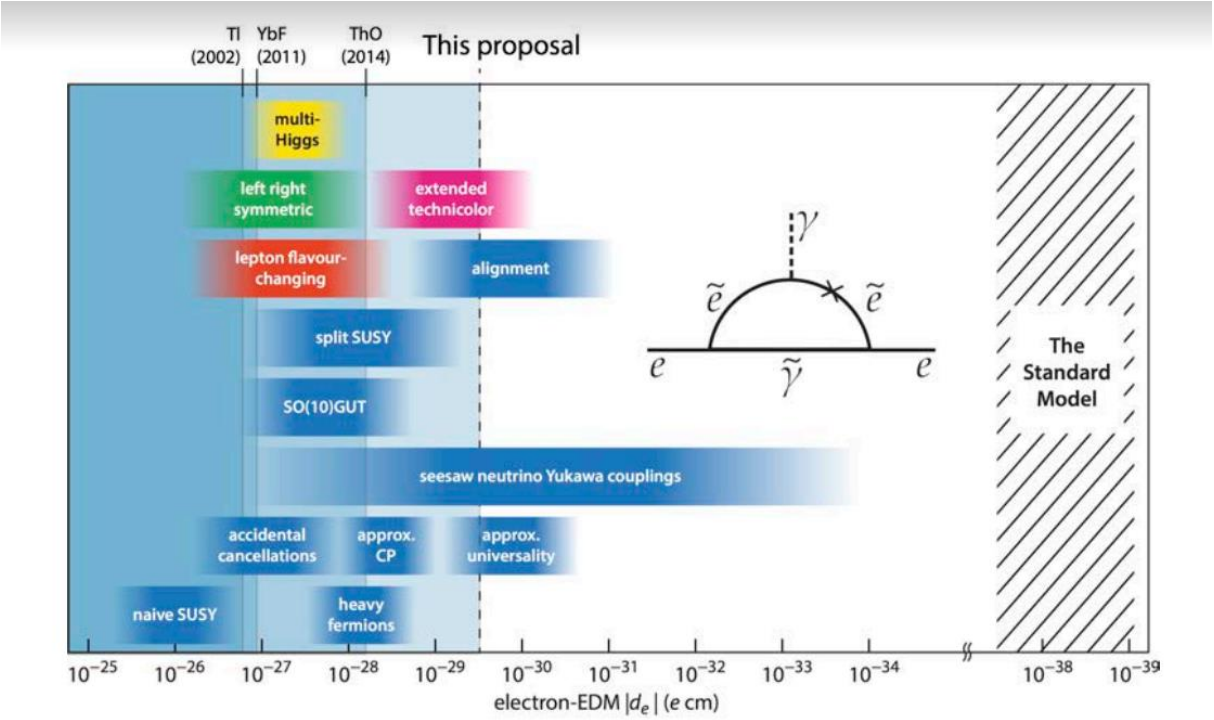

Figure 2: The value of the EDM of the electron, as predicted by various theoretical extensions of the Standard Model, indicated by the colored horizontal bars. The recent experimental upper limits on the EDM, and the reach of the proposed experiment, are also indicated with vertical lines, excluding the shaded regions to the left. The Feynman diagram illustrates a possible EDM arising from the interaction of an electron with supersymmetric particles. Figure taken from [17].

The BaF eEDM search experiment

The advances that have been made in recent years as can be seen in figure 2 and are due to new techniques and the usage of molecules in the search for the eEDM. The supersonic beam of YbF in London [26] and the ThO buffer gas from the ACME collaboration [16] have proven this. For YbF, the interaction energy due to d_e has a relatively high value with respect to previously used atoms like Thallium because of its high internal effective electric field and furthermore the motional magnetic field has a negligible effect [26]. The ThO molecular beam used in the ACME collaboration has an even higher intrinsic effective electric field and an unusual small magnetic moment in its $H^3\Delta_1$ state [16]. In both experiments advantages have been created to measure d_e with great sensitivity.

In the BaF eEDM search experiment though, a combination of advanced techniques is used to measure d_e with an even higher sensitivity. The statistical sensitivity σ_d of an eEDM experiment is given by [17]:

$$\sigma_d = \frac{\hbar}{e}\frac{1}{2\varepsilon_{eff}\tau\sqrt{\dot{N}T}} \tag{2.9}$$

where ε_{eff} is the effective field strength for the valence electron inside the molecule, τ is the coherence interaction time of the molecules with the electric field, $\dot{N}$ is the rate of detected molecules and T the measurement time. However the intrinsic electric field of BaF is considerably lower (6 GV/cm)[27] than YbF (23 GV/cm)[28] and ThO (84 GV/cm)[29], the usage of new techniques enables to manipulate other variables to achieve a high sensitivity. As can be seen from

2.9, the lower intrinsic electric field can be compensated by coherent interaction time, for a given rate of molecules and measurement time. The interaction time is directly connected to the speed in a molecular beam, since the interaction zone has fixed dimensions, therefore in this experiment it is key to slow down the molecules to reach maximum sensitivity.

The schematics of the BaF experiment can be found in figure 3.

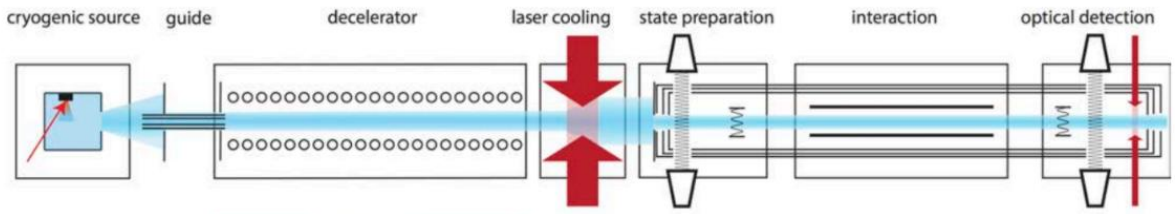

Figure 3: A schematic overview of the BaF eEDM search experiment. Picture taken form [17].

A promising feature of the experiment is to use a cryogenic source [30] for the molecular beam instead of the previously used pulsed supersonic beams, in this way a relatively slow and cold beam (≈ 100 m/s in the longitudinal direction and 60 m/s in the transversal direction) is formed and therefore needs an order of magnitude less deceleration to achieve a τ of 15 ms [17].

The cold molecular beam is guided through a series of quadrupole lenses such that only BaF molecules enter the decelerator. Because of the smaller mass of the BaF with respect to ThO and YbF, the molecules are decelerated more efficiently by the decelerator. The decelerator consists of many ring-shaped electrodes that form a 4 mm tube through which the molecules travel. By the use of traveling wave, or Stark Deceleration, the beam will be slowed down to ±30 m/s for the longitudinal direction. The slow-moving bunch of molecules ejected by the decelerator not only has a narrow distribution of velocities, but also is selected in a single rotational quantum state, and the molecules are spatially oriented, as can be seen in figure 4 [31]. For the purposes of the experiment, a time dependent sinus wave between two different voltages is applied to optimally slow down the N=1 state and N=2 state [32], with optimal decelerating voltages of 5kV and 10kV respectively.

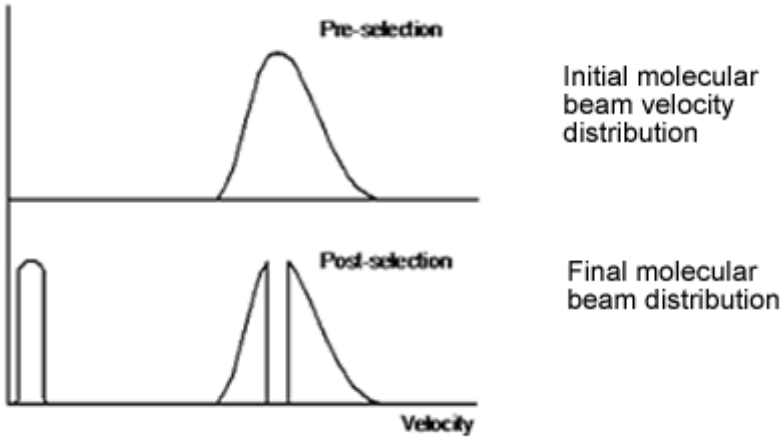

Figure 4: Effect of deceleration on the cryogenic beam.

Now the longitudinal velocity is reduced, the cold beam is led to a laser cooling system to reduce the transversal velocity to ±0.2 m/s. This decreases the divergence of the cryogenic beam. Since the molecules need to be in the N=1 state for the laser cooling, the molecules will be transferred from the low-field seeking states F=2 and F=3 of the N=2 to the F=1 and F=2 of the N=1 state using

25.2 GHz microwave radiation, at the beginning of the laser cooling section [17]. After this first state preparation the beam is cooled with optical Doppler laser cooling. As can be seen from figure 5, the pumping wavelength used is 860 nm (indicated by the straight red arrow), a wavelength for which diodes are available with sufficient intensity. In this figure the branching ratios and the transition dipole moments of the relevant transitions are also given. As can be seen, the probability of electronic excitation is much larger than the probability for vibrational excitation, which makes BaF an excellent molecule to use. Moreover, BaF has a short excited-state lifetime, making it possible to effectively slow down the molecules in a relatively short period of time.

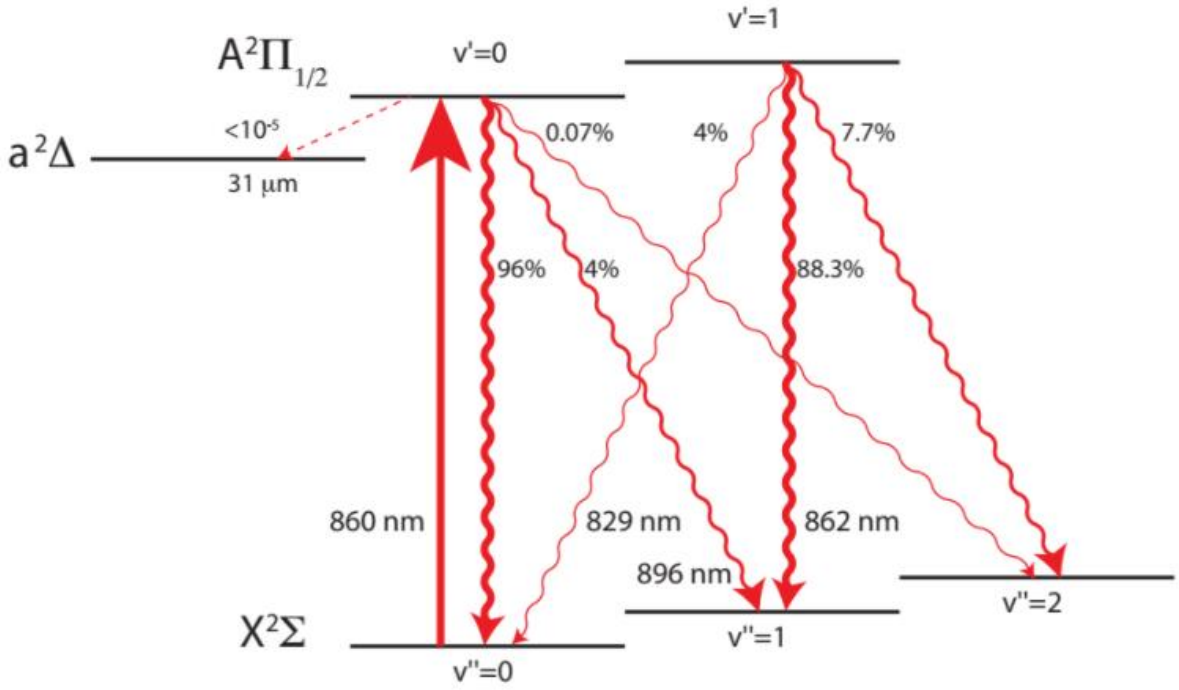

Figure 5: Lowest vibrational levels within the electronic ground state and electronically excited $A^2\Pi_{1/2}$ state of the BaF molecule and its calculated branching ratios. Picture taken from [17].

It is expected that less than 20% of the molecules are lost to other states than the cooling state. After the laser-cooling, the molecules will be optically pumped to a single hyperfine state of the N=1 level, and with the use of 12.6 GHz resonant microwave radiation to the F=0 hyperfine level of the rotational ground state. It is expected that 9×10^5 molecules per shot will leave the cooling section in the appropriate state, proceeding to the interaction zone.

To be able to measure the eEDM, the molecules of BaF will be put in a superposition of magnetic substates. These magnetic substates are acquired by applying parallel and anti-parallel orientations of the electric and magnetic field. In figure 6, the two different states are depicted schematically. As can be seen a phase difference arises from the different orientation, a phase difference directly proportional to the eEDM. This phase difference, φ_{EDM}, is given by:

$$\varphi_{EDM} = \frac{d_e \mathcal{E}_{eff} \tau}{\hbar}, \tag{2.10}$$

where τ is again the coherent interaction time of the molecules with the electric field, $\mathcal{E}_{eff}$ is the effective field strength for the valence electron inside the molecule and d_e the electron electric dipole moment.

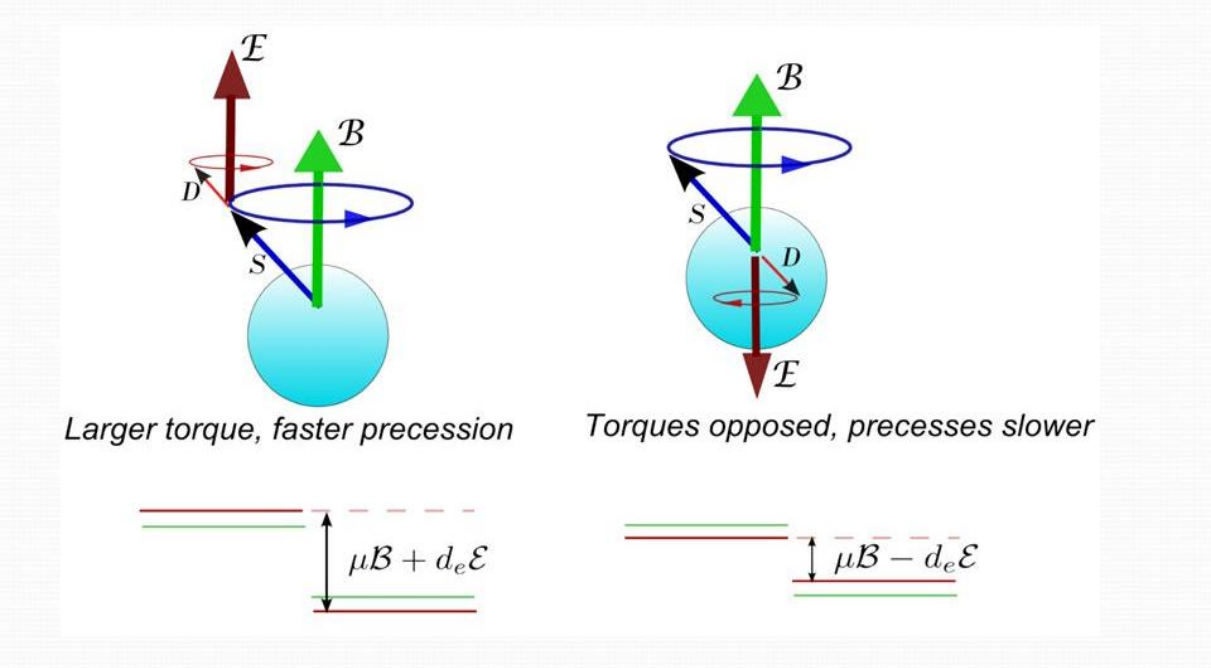

Figure 6: Precession schematics of eEDM with aligned and opposed E and B fields.

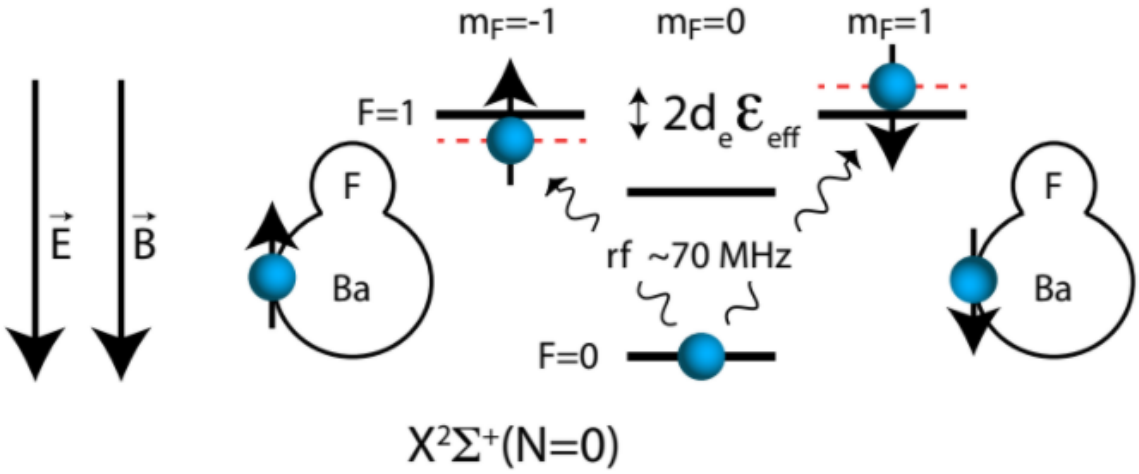

Figure 7: The different orientations, a phase difference is build up making it able to measure the electron electric dipole moment [17].

The Hamiltonian, equation 6, has a dependence on both the electric field and the magnetic field. For this experiment to work, one needs to protect the molecules from magnetic noise. For realistic experimental parameters, the magnetic term in the Hamiltonian is much larger than the electric term, which are both directly proportional to the respective fields the molecule experiences. Therefore, to get a sense of the eEDM, the magnetic field must be very small and constant. To have a Larmor precession of $\pi/4$ in the interaction zone a field of 600pT is needed [17]. The experiment depends on good contrast and thus depends on the accumulated phase difference. Using a field of 600 pT will enable to measure the first fringe increasing the accuracy of the measurement.

An inhomogeneous field will cause differences in the magnetic precession rates of the molecules. When this difference is too big the the precision of the experiment will go down, by dephasing between different parts of the interaction zone. Calculations have shown that for this

measurement specifically the relative magnetic field difference, for which the molecules' mutual spin angle difference is less than $\varphi = \pi/2$ is when $\delta\mathbf{B} < 3.154$ pT for a field of $|\mathbf{B}| < 50$ pT, [33] the aim for the field strength of the BaF eEDM search experiment. The interaction zone is 0.5 meter long, together with the state preparation and optical detection zone, the field needs to be compensated to this extend for 1 meter.

Magnetic compensation and stabilization

There is no such thing as a zero magnetic field, since there are no magnetic monopoles [18]. Furthermore magnetic fields are the consequence of moving electrical currents, which in everyday life is impossible to get around. Since these are the reals, to achieve "zero magnetic field" an option is to create a field exactly opposite to the external magnetic field, to achieve a net zero field, compensation of this type is called active compensation. This compensation however will not be perfect, but can reach a level considered to be sufficient, for the BaF eEDM search experiment this yields $|\mathbf{B}| < 50$ pT.

To actively compensate a region it is necessary to know the magnetic field in the region of interest. It is therefore wise to subdivide different sources to the total external magnetic field. The biggest part of the external magnetic field is the earth's magnetic field, which is typically of order 0.5 Gauss [34]. However, this magnetic field is really susceptible to distortions. Every metal object has influence on the local field, therefore, since e.g. buildings have a metal structure the earth magnetic field is distorted in normal laboratory facilities and can differ strongly locally.

Yet, to actively compensate a *homogeneous* field one can think about using Helmholtz coils [35,36]. Such a system is depicted in figure 8. Making use of two identical coils placed symmetrically along one axis, at a distance equal to their radii, a linear field is generated when two equal currents are carried in the same direction.

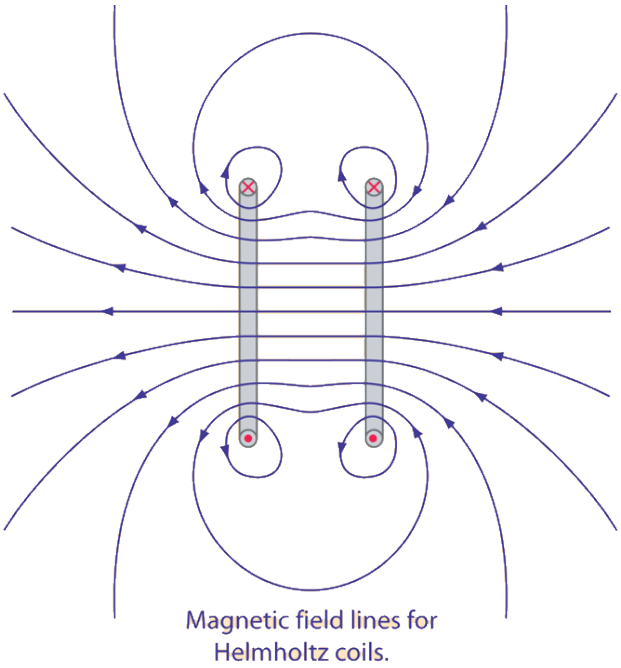

Figure 8: A schematic figure of Helmholtz coils with its magnetic field lines.

Due to the current through the wires, a magnetic field is generated (figure 9). The centre of the coils, picks up a magnetic field equally generated from all directions, creating a linear field along

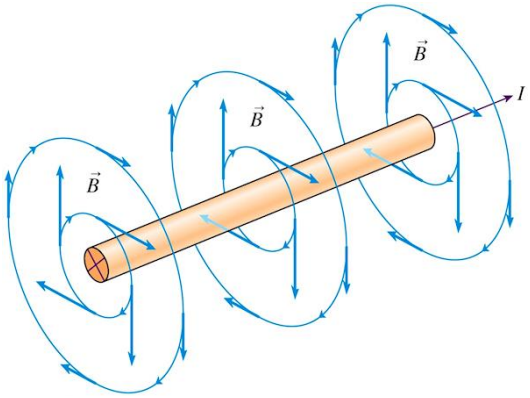

Figure 9: Magnetic field around a simple current-carrying wire.

the central axis. Yet this field is not perfectly homogeneous. Moving along the central axis the magnetic field strength in the plane of one coil differs about 5% per cent with the magnetic field strength in between the two coils. As can be calculated from a single wire loop with the use of the Biot-Savart law, yielding [18]

$$\boldsymbol{B}(x,R) = \frac{\mu_0 I n R^2}{2(R^2+x^2)^{3/2}}, \tag{2.11}$$

where μ_0 is the magnetic permeability of free space, I the current through the wires, n the number of wires and R the radius of the loop, using a superposition of two loops with for the field in the plane of a coil $x = 0$ and $x = -R$ and for the centre $x = R/2$ and $x = -R/2$.

Though, when moving in the plane of one coil, it is mainly the orientation (to 2nd order) of the field that is changing, since distance to the wire is not evenly distributed. The closer to a part of the loop, the more curvature there will be in the magnetic field, as predicted by Ampères Law. Therefore the field, with the corresponding direction and curl, in between the Helmholtz coil at an arbitrary point is hard to determine and strongly depends on several specifications of the system.

One of the advantages of using electrical systems as magnetic shielding is that the current, and voltage, is usually easily adjustable. One could therefore not only compensate the external field but use a feedback system like in figure 10, to stabilize the resulting field [35]. Compensation of this kind is called active dynamical magnetic compensation.

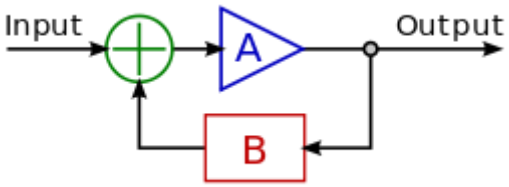

Figure 10: A typical feedback system. For our purposes A represents an electrical system, the output is represents the magnetic field, B a magnetometer, which gives feedback in such a way that by current control the magnetic field is stabilized.

As the active compensation is described by one of the two sources of magnetic fields [19], the electric current, the passive compensation is advantageously using the other source of magnetic fields, the spin magnetic moments of elementary particles. In most bulk materials there is a net magnetic moment only if there are atoms present whose inner electron shell is not filled. Then there can be a net angular momentum and a magnetic moment. Such atoms are found in the "transition element" part of the periodic table, for instance, chromium, manganese, iron, nickel, cobalt, palladium, and platinum are elements of this kind. When these metals are placed inside a magnetic field, the magnetic moments will be lined up in the direction of the field and the material is said to be magnetized.

The degree of the ability of a material to support the formation of a magnetic field within itself is called permeability. In metals, the exclusion principle can be disobeyed for two by the magnetic field aligned electrons next to each other, since there are free electrons flying by with the opposing spin. An alloy with a particular high permeability is Mu Metal [37], made from primarily nickel and iron. When a structure of this material is placed around an object therefore, the external magnetic field tends to interact with the metal, with the consequence that a path is created around the object inside this material, making it able to shield the inside object from the magnetic field, as is depicted in figure 11.

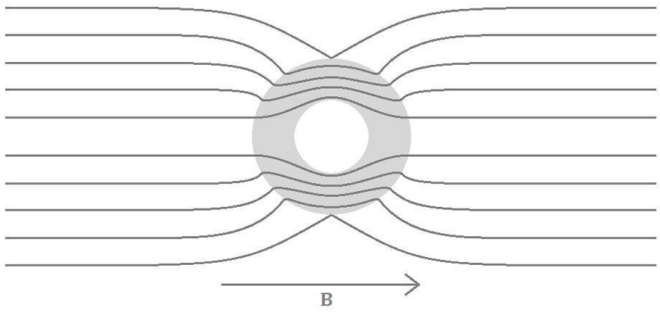

Figure 11: Magnetic field lines interacting with a mu metal infinite cylinder. Picture from [38].

For shielding purposes, several problems come up with the use of mu metals. As the field exceeds a certain limit, the material gets saturated and the shielding has come to a maximum. Moreover, at low field strengths the materials permeability can drop off, reducing its effect. It is therefore important to use a set of such materials to achieve maximum shielding. However, materials of such type can be expensive.

For optimal magnetic shielding it thus is key to use a combination of active and passive shielding.

3. Set-up

To examine the active compensation a 3 dimensional cubic Helmholtz-like coil configuration is used. The configuration can be found in figure 12. The configuration is fully symmetric and has dimensions 62.0(1) x 62.0(1) x 62.0(1) cm. It consists of six coils, with two opposing coils connected to the same power supply, creating three individual Helmholtz-like coils. The current carrying wires (~20-25 per coil) are depicted in black, the skeleton in grey. The skeleton is made of aluminium and is exactly cubic. The bundle of wires has a cross-section of 1.0(1) x 0.5(1) cm and is wounded roundly around the corners with a radius of 1.0(1) cm.

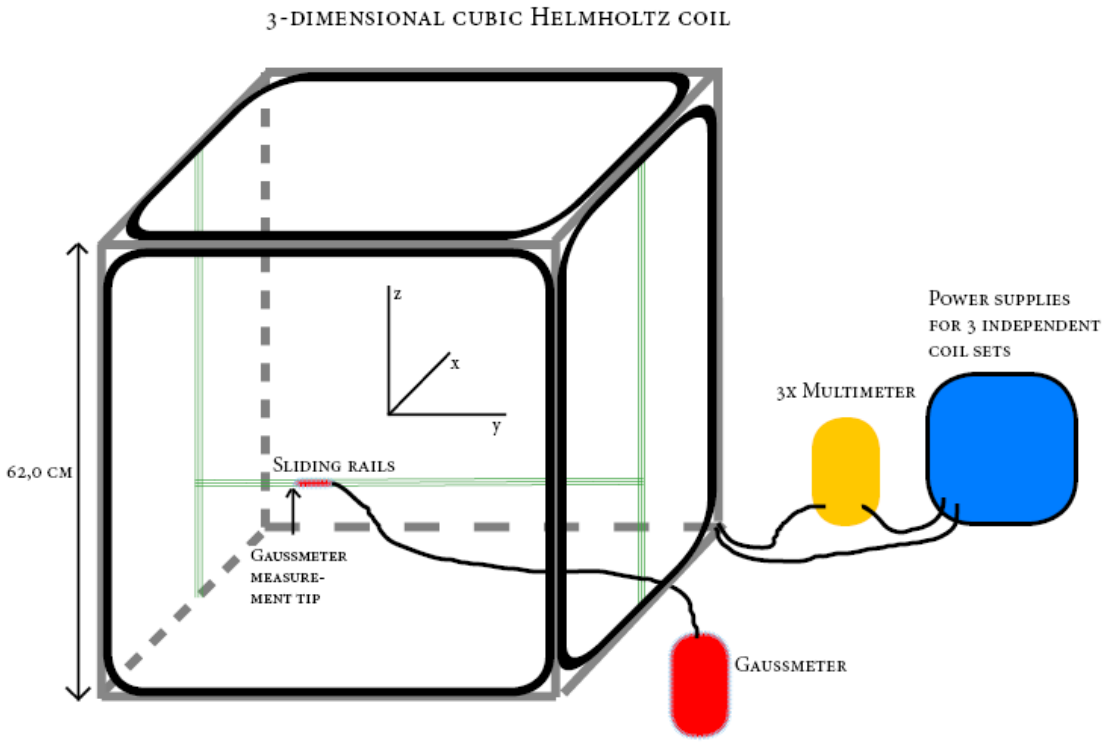

Figure 12: An illustration of the 3-dimensional cubic Helmholtz-like coil configuration as was used in the experiments.

The power supplies have changed over subsequent measurements for sake of improvement of the measurements. At first, two Bench power supplies, type CS13003XIII, ranging to ±3A were used. When one of the output signals had proven to be inaccurate, a 0-15V / 2A EPro PS1502A with analog current stabilization was added to replace this output. For more stable and precise currents a laser diode controller LDC500 from ThorLabs was used, however this precision was at the expense of the range of the current controller, which is limited at 500mA. The latest experiments were executed with a 3 channel HMP2030 Rohde & Schwarz 0 V to 32 V/0 A to 5 A (188 W) power supply. To measure the current through the coils and note consistency with the power supplies, three Ampere meters were placed in series with the coil sets.

To measure the magnetic field an AlphaLab Inc. Vector/Magnitude Gaussmeter model VGM [38] was used, ranging from 0.00 to 800.00 Gauss for the magnetic field magnitude and being able to measure the magnitude and direction of three orthogonal components. This instrument consists of a display and mode part, and a probe to measure the magnetic field. The probe consists of a metal bar of 6.35x6.35 mm cross section and is 50 mm length. The probe measures the field with three Hall sensors placed within 3.2 mm from the tip, therefore at the end of the bar a miniscule triangular inset is visible. The accuracy of the probe is ±1% for all individual components as for the magnitude, yet the noise level is 0.02G. For our purposes this noise is important and is relatively big compared to the given accuracy of AlphaLab. The total error is described by:

$$\sigma_{total} = \sqrt{\sigma_{noise}^2 + \sigma_{accuracy}^2 + \sigma_{statistical}^2} = \sqrt{(0.02\text{G})^2 + (1\% * B_i)^2 + \left(\frac{B_{i,max} - B_{i,min}}{N}\right)^2}, \quad (3.1)$$

where σ is the respective error, B_i the magnetic field component for $i = x,y,z$ or the field magnitude and N the number of measurement points. The statistical error is only relevant for results where a Gaussian distribution is expected and is taken to be 0 otherwise. An extra feature of the Gaussmeter is the reset function, which sets the current field as zero, making it easy to measure induced fields.

To measure the spatial dependence accurately, inside the configuration a set of aluminium slides was placed. This enabled to securely measure the magnetic field and its individual components and ensured the orthogonality of the configuration was in line with the orthogonality of the probe. For several measurements, different coordinates were measured, these were always indicated on the slides, to ensure repetitive stability. The origin of the coordinate system is at the centre of the configuration, with the directions as depicted in figure 12. Since the sensors are placed on the tip of the probe it was impossible to measure an extreme value without changing the direction of the probe, or the configuration of the slides. For the measurement of these extreme values it was decided to turn the slides clockwise, making it easy to repeat the measurement for several coordinates in the extreme coordinate plane.

A Helmholtz coil consists of two circular identical coils placed at a distance equal to their radii from each other (see section 2.3). The configuration used in this experiment differs from the 'perfect' Helmholtz coil in two fashions. Firstly, the distance two opposing coils are placed apart is not equal to the distance of the radius, the distance apart is equal to the base, although not applicable to squares, two times the radius. Secondly, the coils used are not circular but (almost) square. As a consequence, the generated field has a character more like the field around a single wire (figure 9), especially at the centric extreme values, than a 'perfect' Helmholtz coil would have.

4. Measurements and results

Qualitative zero field measurement

To map the problems to uncover for compensating the magnetic field a qualitative measurement was conducted. This first measurement was a measurement of the magnetic field when all coils were set to compensate for the magnetic field at the centre of the coil, and was conducted by measuring the individual components. This meant that there was a compensation of 0,04(2)G, 0,32(2)G and -0,33(2)G for the x, y and z axis respectively. For this compensation a current of 0,19(3)A, 0,21(3)A and 0,74(3)A was used, though as mentioned in chapter 3, the power supply for the y-direction was not reliable. Per spatial coordinate the field was measured in all directions. The spatial coordinates used were x = {-25,0,25}, y = {-14.5,0,14.5,29} and z = {-31,-14,0,14,25.5}, where all coordinates are in centimeters, which will be consistent throughout this thesis. The choice for the coordinates was purely made by logistical reasons. For these measurements first all the coordinates on the x = -25 cm axis were measured, subsequently the x = 0 cm axis a day later the x = -25 cm coordinates were covered. Because of the time-dependent external magnetic field [33], the currents needed to be adjusted to 0,26(3)A, 0,37(3)A and 0,69(3)A respectively for a zero magnetic field in the centre of the configuration.

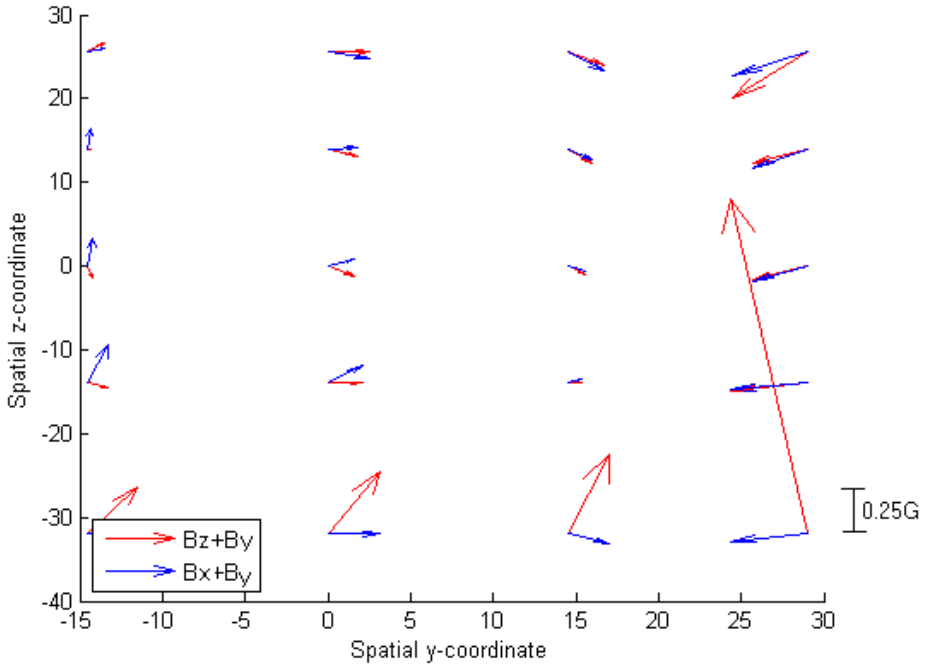

Figure 13: Magnetic field strengths in the x=-25 plane for the first zero measurement. Bz is the vertical component of the red arrow, Bx the vertical component of the blue arrow. By is depicted horizontally. The axis show the y- and z-coordinates in cm.

The magnetic field at x = -25 cm is given in figure 13. One can see there are a lot of deviations in the field. At the corner, y = 29 cm, the Gaussmeter is close to the current carrying coils causing a large magnetic field from one wire (figure 9), with the most extreme value of B_z = 1.70(4)G = 3,5 B_E. At y = 0 cm or z = 0 cm the magnetic field is merely compensated to orders of tenth of B_E.

Thus, it is important to look at the results of the x = 0 cm plane given in figure 14. In this plane there is better compensation. Near the centre, depicted in the grey box, the components are

varying from -0.10(2)G to 0.08(2)G, with 11 out of 18 components having $|B_i| < 0.05$G, a tenth of B_E.

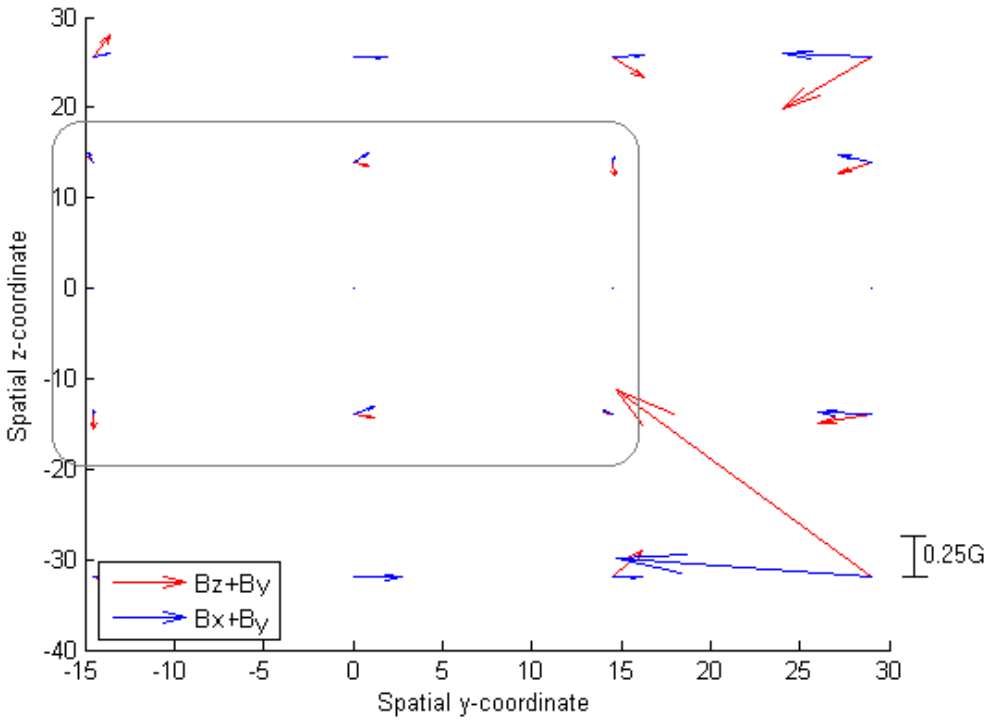

Figure 14 Magnetic field strengths in the x=0 plane for the first zero measurement. Bz is the vertical component of the red arrow, Bx the vertical component of the blue arrow. By is depicted horizontally. The axis show the y- and z-coordinates in cm.

Due to the fluxgate that was placed in the centre, the rail of the set-up couldn't be placed in the xy-plane, and measurements couldn't be done. Again is observed that the ultimate values are too close to the coils and pick up the circular field around one wire. Overall, the field strength is lower for the x = 0 cm plane than for the x = -25 cm plane.

The measurement from the x = 25 cm plane, shown in figure 15 at page 19, show a similar result as that of the x = -25 cm plane. However, B_x has switched signs, which is the most clear for the y > 0 cm components.

For the subsequent experiments the set-up has been improved. It was noticed that not all the power supplies gave a steady current, and experiments should be conducted to check if a steadier power supply would yield a steadier compensation. Moreover, to have a double check on the applied currents, three Ampere meter were be placed in series with the coils. Also, to investigate the region of interest the fluxgate was removed. With these changes in the set-up, a better map of the centre of the configuration can be made. Since the region of interest finds itself in the centre of the configuration, and not at extreme values, measurements near the centre will give valuable information. Moreover, it is handy to take symmetric coordinates, in this way a better map of the behaviour of the magnetic field can be made.

With these results, an indication is given of how the field behaves, like the switch of the sign of B_x when x is below respectively above x = 0 cm. Yet, an exact symmetric results should have been

obtained. Therefore it is key to investigate the stability of the external magnetic field with respect to the spatial coordinates. If there is a clear observation that the external field varies with the coordinates, better understanding of the configuration and the test lab can be made. To limit the error from the variation of the external field, it is necessary to execute the measurement faster, as in this experiment it is observed that a different day yielded a different external field. The reason for the difference in the external field is not directly clear, yet it was readily investigated that in normal working hours, the instability of the field of about 100nT [33], which translates to 0.001G and is negligible to the noise of the Gaussmeter (0.02G+1%**B**).

Moreover, following measurements can be done only in a central plane. This will save time, reducing the time-dependent error and still conclusions can be drawn by symmetry. Though, it should be investigated how the field behaves when one current is applied for one direction, and how the effective field is oriented. In that way it is possible to construct the off-diagonal magnetic field information in one dimension, and superpose it to obtain the effect in three dimensions, since the three dimensions are invariant.

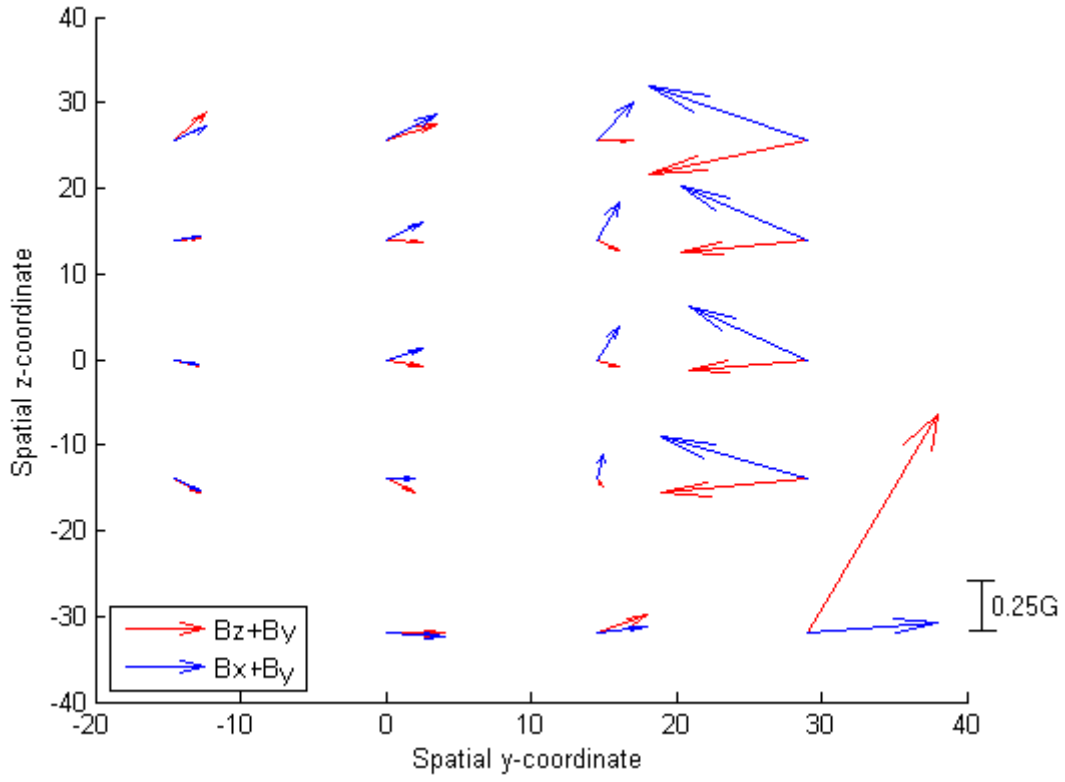

Figure 15: Magnetic field strengths in the x=25 plane for the first zero measurement. Bz is the vertical component of the red arrow, Bx the vertical component of the blue arrow. By is depicted horizontally. The axis show the y- and z-coordinates in cm.

Measurement of the Coil Constant

With an improved set-up the coil constant was measured. The improvement yields the change of two power supplies, the EPro PS1502A and LDC500 were integrated to the set-up. The coil constant is defined as the change of the magnetic field strength over the change of the applied current:

$$C = \frac{d\boldsymbol{B}}{dI} \tag{3.1}$$

Therefore, the magnetic field strength is measured per individual coil for a set of 10 evenly spaced different currents, the slope of the resulting values will point out the coil constant.

For this measurement the reset function of the Gaussmeter was used. The Gaussmeter was placed in the centre and all axes are measured separately. Because in the new set-up three different power supplies were used, the range and precision is different for all directions. To elaborate on this, the LASER-current supply is the most precise, but is limited to a value of 500mA, while the CS13003XIII has a maximum of ±3A, but has a smaller precision. Furthermore, for the power supplies, the value is always double-checked by using an ampere-meter in series with the connected Helmholtz coil, when deviations between the two occurred, the value presented by the ampere-meter is regarded as the real value. There were only deviations between the two values for the CS13003XIII, these deviations were consistent.

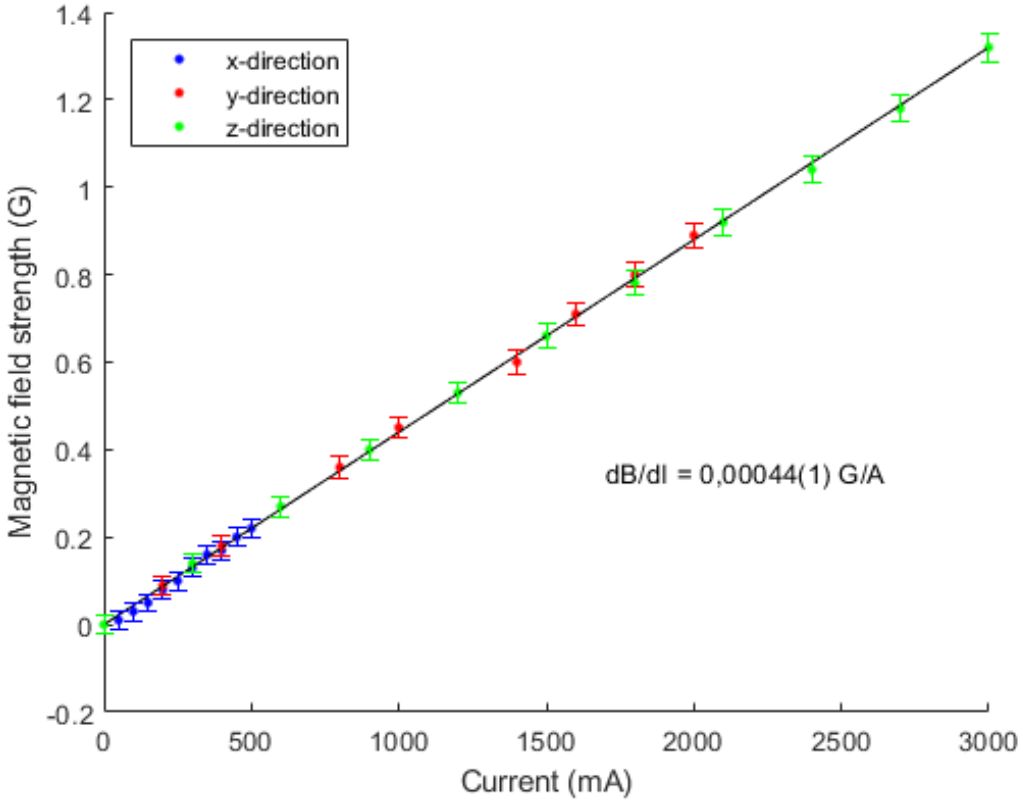

Figure 16: Measurements of the field strength with various currents applied. The measurements were executed for three directions individually. Also the coil constant, the best fit slope, is given in the figure. The error is equal to the noise of the Gaussmeter plus 1 per cent of the measured value.

In figure 16 the results of the measurement are given. The magnetic field shows a linear dependency on the applied currents. Therefore the slope of the graph gives the coil constant. The coil constant is 0,44(1) G/A. For all three directions, though for different intervals, the coil constant is equal and the line goes through all measured values. It can thus be concluded that the coils are identical, which indicates for the future of the experiment that theory can be applied in the same manner for all directions.

Measurement of the external magnetic field

As was stated in the discussion of the first measurement, spatial fluctuations of the external field are unknown. Therefore it is important that this is measured. Since magnetic fluctuations occur near all magnetic objects, it is not necessarily a fact that the external magnetic field is locally constant. To give a feeling, the magnetic field near a tip of a screwdriver is over five times the earth's magnetic field, the field decreases with distance. During all measurements all magnetic objects, were placed at least one meter from the coil. One meter was measured to be enough in a quick measurement, making it cause no fluctuation in the field.

For measuring the external field the Gaussmeter was placed in the rail and a 3D map of the background field was measured, with x = {25,0,-25} and y = {25,12.5,0,-12.5) and z = {25,12.5,0,-12.5,-25}, where all coordinates are in centimeters. At all points, B_x, B_y and B_z were measured independently. The results are given in figure 17, 18 and 19 for these directions respectively. The results are depicted in a graph with on the y-axis the magnetic field strength, B, in Gauss. The x-axis has no label since there appeared to be no spatial influence. For completeness, in the figures there are five sets of four points with three different colours. As the legend shows the different colours describe the different x-planes. The first four points show the results for z = 25 cm, whereas the last four points show the results for z = -25 cm. The y-coordinates are ascending. The error bars are equal for all points and given in the spacings.

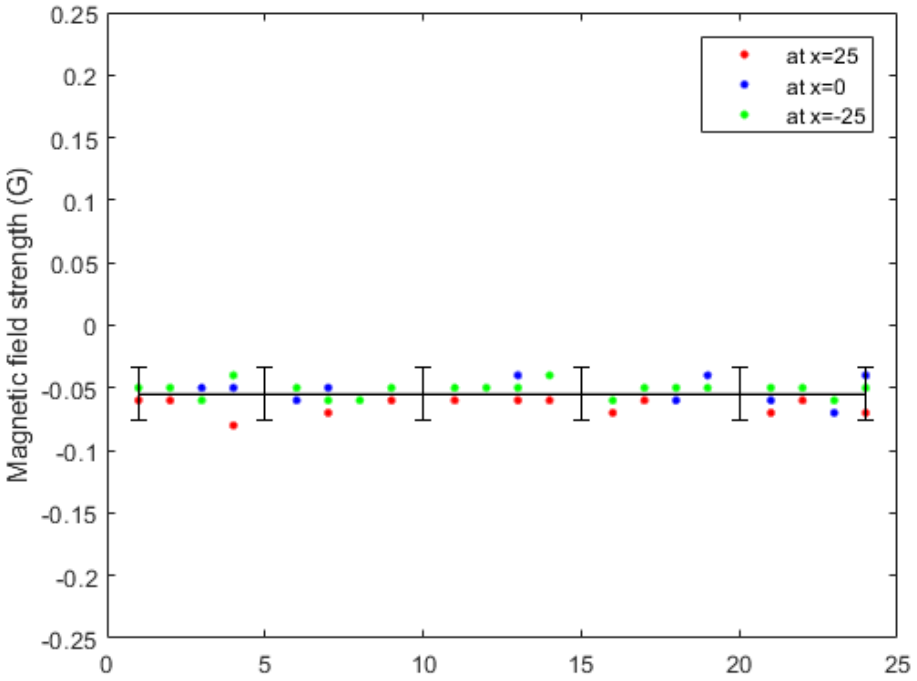

Figure 17: The x-component of the external magnetic field. The first four points are at z = 25 cm with ascending y. The last four points are at z = -25 cm.

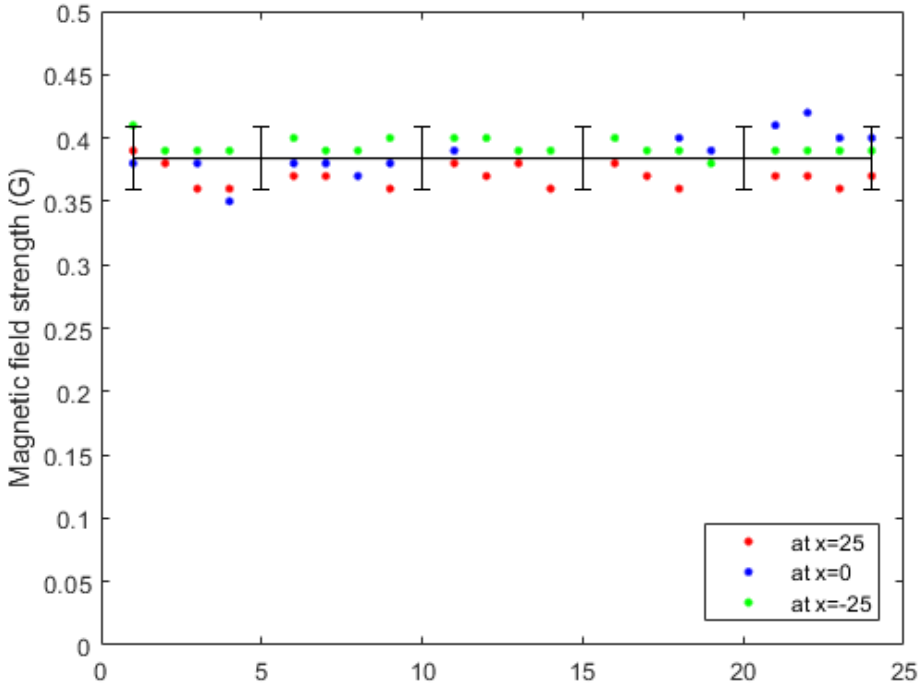

Figure 18: The y-component of the external magnetic field. The first four points are at z = 25 cm with ascending y. The last four points are at z = -25 cm.

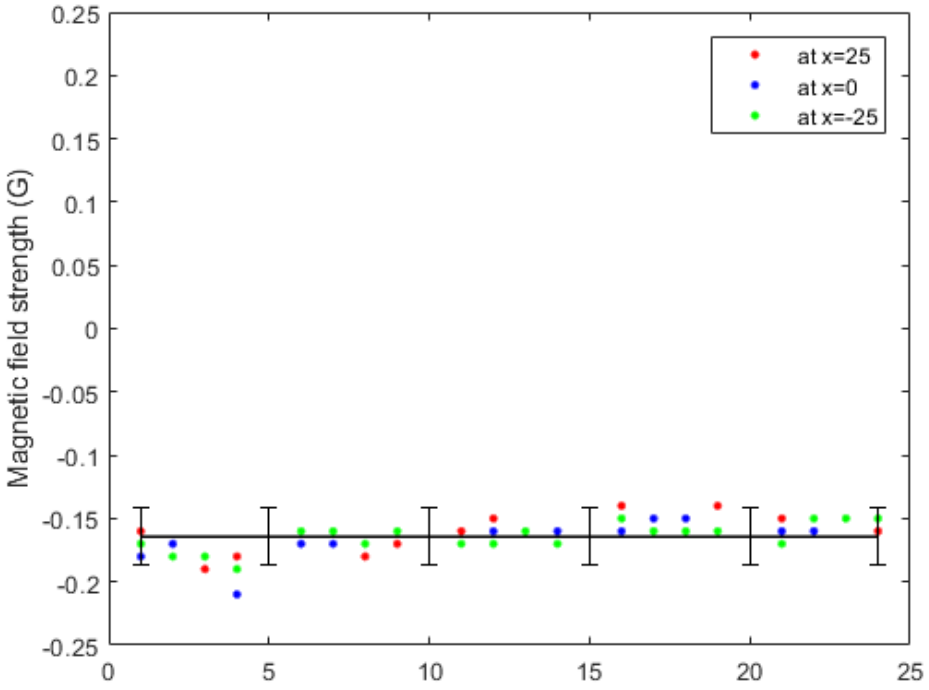

Figure 19: The z-component of the external magnetic field. The first four points are at z = 25 cm with ascending y. The last four points are at z = -25 cm.

For this measurement the external field is composed out of B_x is -0.05(2)G, B_y is 0.38(3)G, B_z = -0.16(2)G, making:

$$\boldsymbol{B}_E = \begin{pmatrix} -0.05(2) \\ 0.38(3) \\ -0.16(2) \end{pmatrix} \text{G},$$

where the errors are obtained using equation 3.1, including the statistical error to account for the slight fluctuations. It is concluded that the external field is locally stable even though these slight fluctuations are observed. This conclusion of local stability is strengthened by the fact that no clear relation can be obtained between the slight fluctuations. Moreover, an analysis of the total field shows that the total field is stable with a better precision than the combined error. The total field, mathematically calculated, in this measurement $|\mathbf{B}|$ has a bottom value of 0.40G and a top value of 0.44G with a mean of 0.42G. Thus $|\mathbf{B}|$ is 0.42(2)G, yet the combined error of the components yield an error of 0.04G. Since the error in the total field is smaller than the combined errors of the components, it can be concluded that the background field is spatially stable.

The magnetic field stability of one Helmholtz-like coil set

To understand better what the spatial dependence of the magnetic field is when using this Helmholtz-like coil configuration, the induced field was measured if one current is applied. To reduce the relative background noise a strong field was applied. Therefore the focus lies on the z-axis which was connected to the most powerful power supply, ±3A. Because we are interested in the variation of the field, how much it differs from homogeneity, the reset function is used to cancel out the other components, before switching on the coil. This is allowed since the external field is stable, and therefore will not give rise to systematic discrepancies. In this measurement the magnetic field is measured in 2 planes, the y-plane and the x-plane, for all components. In this manner it can be measured to which extend, for example inside a cylinder with r=R/2, the field is homogeneous. Moreover, the measurement of two planes provides for comparing both results, which are expected to show the same, yet opposite, pattern, since the y and x axis are interchanged, the B_x and B_y should as well. Per plane 25 measurements were done, ranging from -25 cm to 25 cm in 5 steps of 12.5 cm per axis. The coordinates are in centimeters and will be denoted dimensionless in the text for brevity.

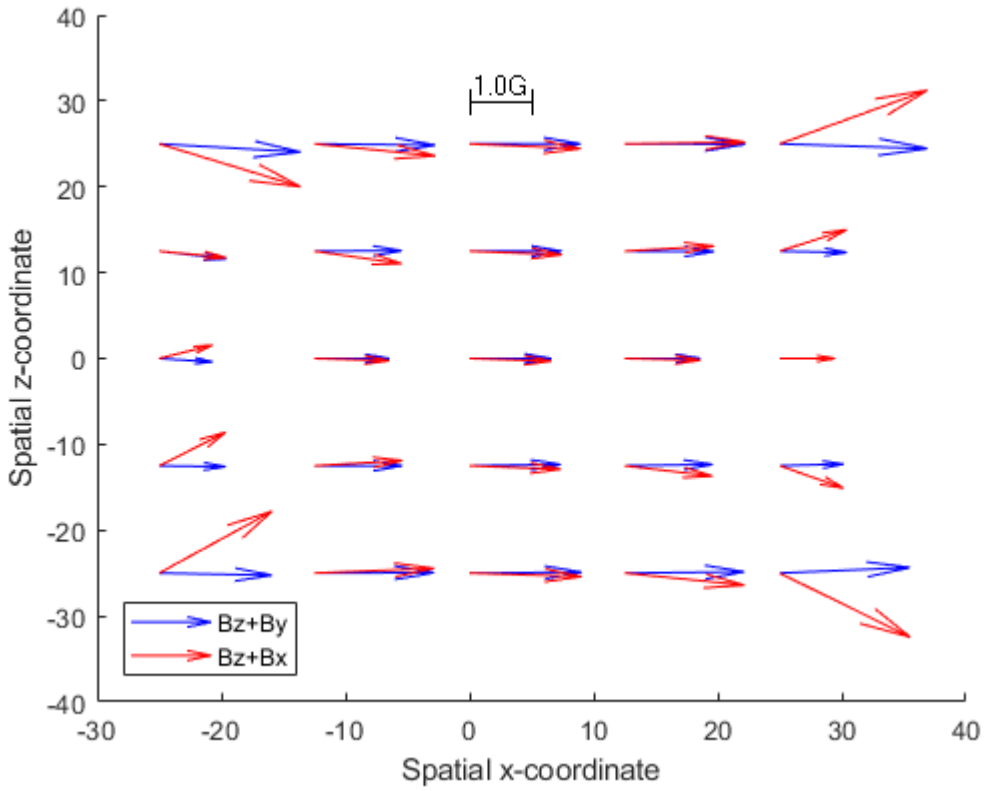

Figure 20: The strong magnetic field measurement of the y-plane at y=0. The vertical component of the blue arrow gives the y-component of the magnetic field, as does the red arrow show the x-component. The horizontal component is the field in the z-direction of the field. The axis show the x- and z-coordinates in cm.

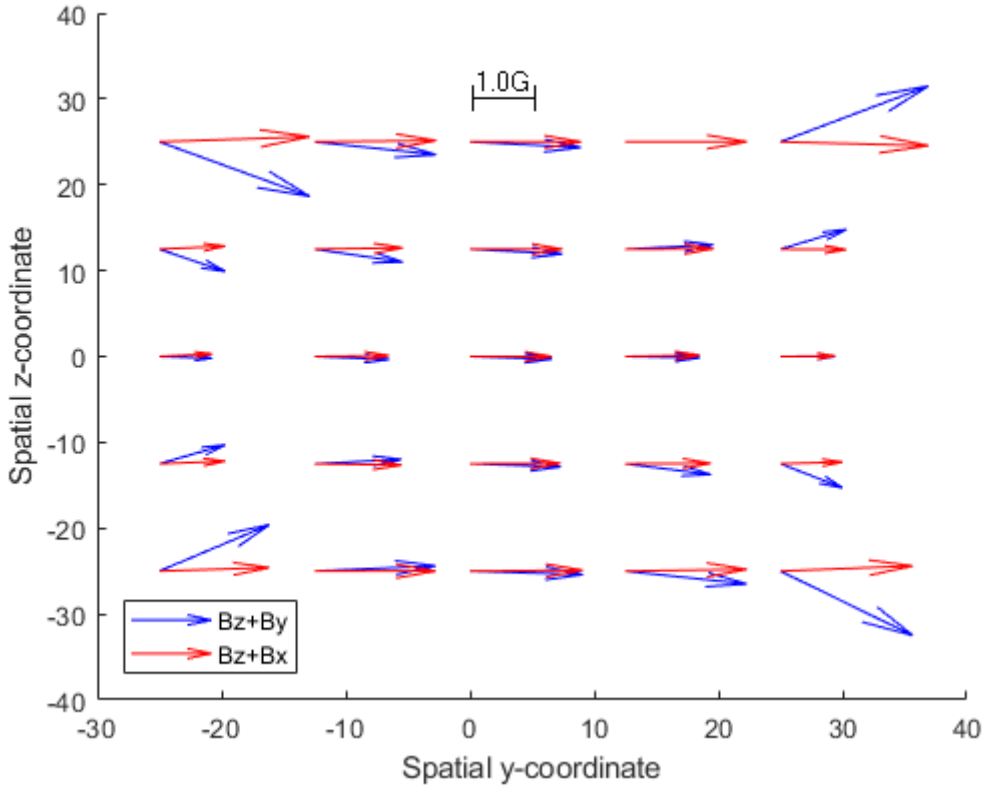

Figure 21 The strong magnetic field measurement of the x-plane at x=0. The vertical component of the blue arrow gives the y-component of the magnetic field, as does the red arrow show the x-component. The horizontal component is the field in the z-direction of the field. The axis show the y- and z-coordinates in cm.

In figure 20 and 21 the results are presented. Figure 20 depicts the field in the y-plane. The horizontal component depicts the z-component of the field, which is the biggest component, since the coil generating a field in the z-direction is switched on. In the centre the z-component has a value of 1.32(3)G. This centre value will be denoted by $B_{z,0}$. The figure shows that the z-component and the total field strength decrease when moving from the centre along the x-axis. On the x-axis, the field is linear, though at (-25,0) a B_x is measured of 0.31(2)G is measured, which is a significant value. Both y-sides of the square coil, generate a field in the x-direction, but by symmetry these should cancel out.

For locations outside of the x-axis, the current on the wires induce a relatively large field, see figure 9, therefore not only B_z increases but B_x as well, in the y-plane B_y stays zero except for the extreme coordinates where it picks up a factor $B_{z,0}/10$. Moving along the z axis, the z component of the magnetic field tends to increase. Figure 20 and 21 show the same dependency, with B_x and x directly interchangeable with B_y and y. Moreover, B_y does stay zero along the y-axis.

To define a region of interest the compensation factor must be examined. The region of interest is defined to be the region where the field is stable to a level of 10 per cent or less. All measured field components are a direct product of the induced field in the z-direction and therefore the compensation factor at a point is calculated by the field strength at a given point, minus the value in the particular direction in the spatial centre divided by the field strength in the z-direction at the centre, giving us stability factor or compensation factor, called c_i:

$$c_i = \frac{B_{i,r} - B_{i,0}}{B_{z,0}}, \tag{3.2}$$

with $B_{z,0}$ = 1.32G. In figure 22 and 23 the results are presented. One can see that the component of the field is constant in its plane, therefore we can conclude that the region of interest is invariant to this plane, using one coil. For the perpendicular component (22b and 23c), there are peaks in the corners, a positive peak at (-25,-25) and (25,25) while the field is opposite at (-25,25) and (25,-25), with (x,z) and (y,z) coordinates respectively. To examine the region of interest three points of figure 22 are considered. Point (12.5,12.5) gives a stability to 13(3)%, and just outside the region of interest, while at (12.5,0) the field is stable to 2(3)%, at (25,0) the field is stable to 5(3)%. The stability of the compensation of the field has the form of a '+', in the horizontal and vertical direction there is almost no induced field. Whilst at the cross-axes the field is induced, picking up the radial field from one wire.

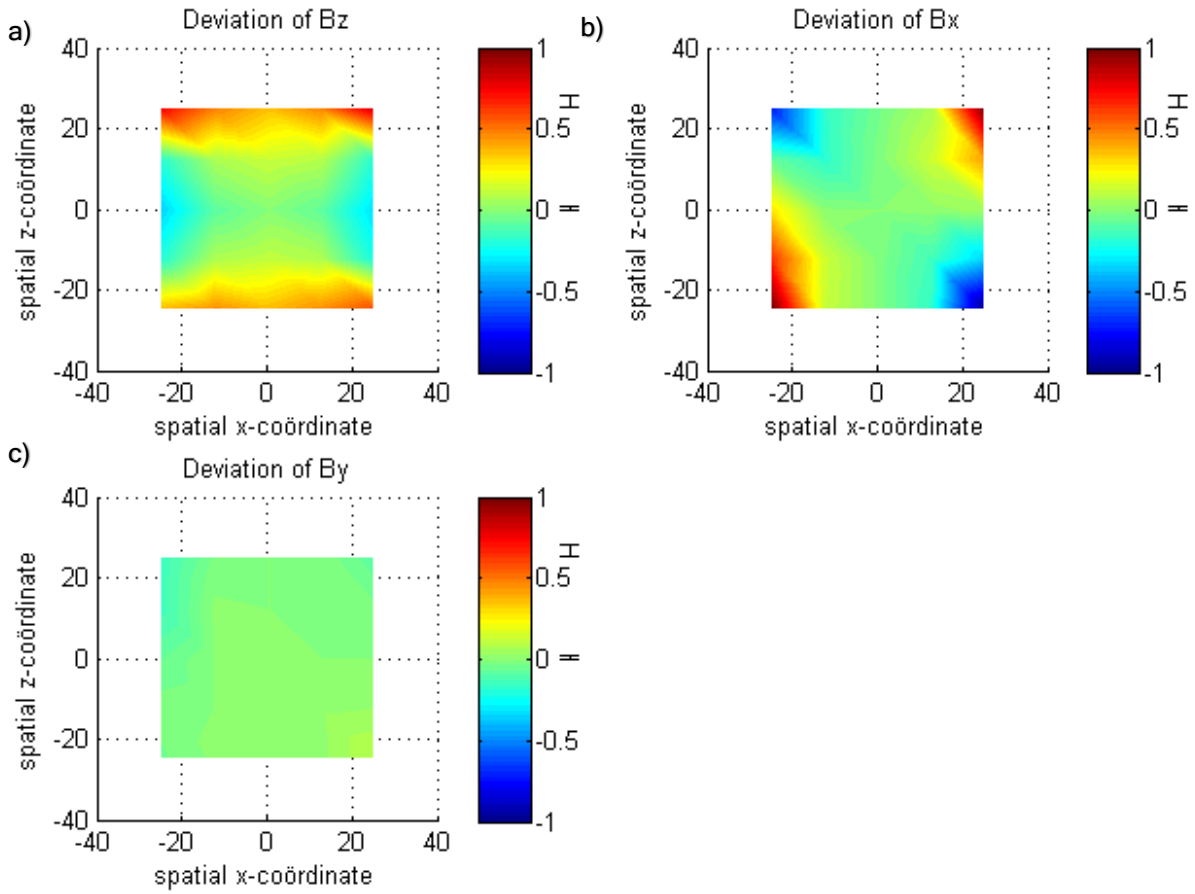

Figure 22: The compensation factor of the field given per component for the y-plane with a large field applied in the z direction. The axis show the x- and z-coordinates in cm. a) gives the compensation factor for the z-component, b) for the x-component and c) for the y component.

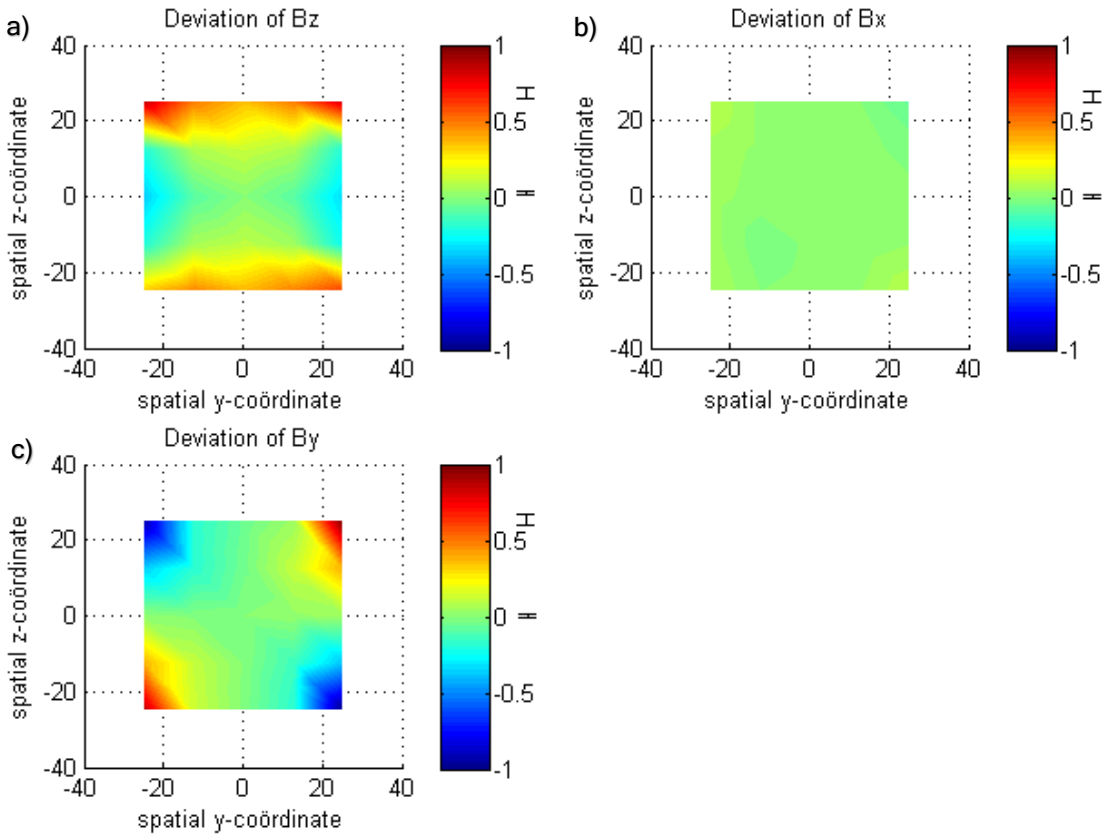

Figure 23: The compensation factor of the field per component for the x-plane with a large field applied in the z direction. The axis show the y- and z-coordinates in cm. a) gives the compensation factor for the z-component, b) for the x-component and c) for the y component.

For the z-component the same analysis can be applied. The z-component has the largest deviations at the north and the south side, as can be seen clearly in figure 22 and 23. To get boundaries to the region of interest let's consider the same points as before. At (12.5,12.5) the stability is to a level of 9(3)%, and is therefore inside our region, while at (12.5,0) the field is stable to 13(3)%, which is thus outside our region. Since the y-component has it's stability in the '+' shape, the z-component has better stability in an 'x' shape. The best way to see this is to look at the left corner of the Bz component of figure 22 and 23, where a '>' shape contour is observed.

To ensure stability of all components, one should therefore be in the centre of both the 'x' and the '+' shape creating a square with a length of about 10 cm for a cubic helmholtz coil of 62 cm. Yet for the BaF eEDM search experiment the field magnitude, rather than its orientation is what matters. In figure 24 the graphs of the compensation factor for the field magnitude is given. Note that since the magnitude is used, all compensation factors are positive. A square with a radius of 10 cm would be inside the region of interest, for this interpretation. Therefore there needs to be done further investigation with a larger set of points in a smaller region.

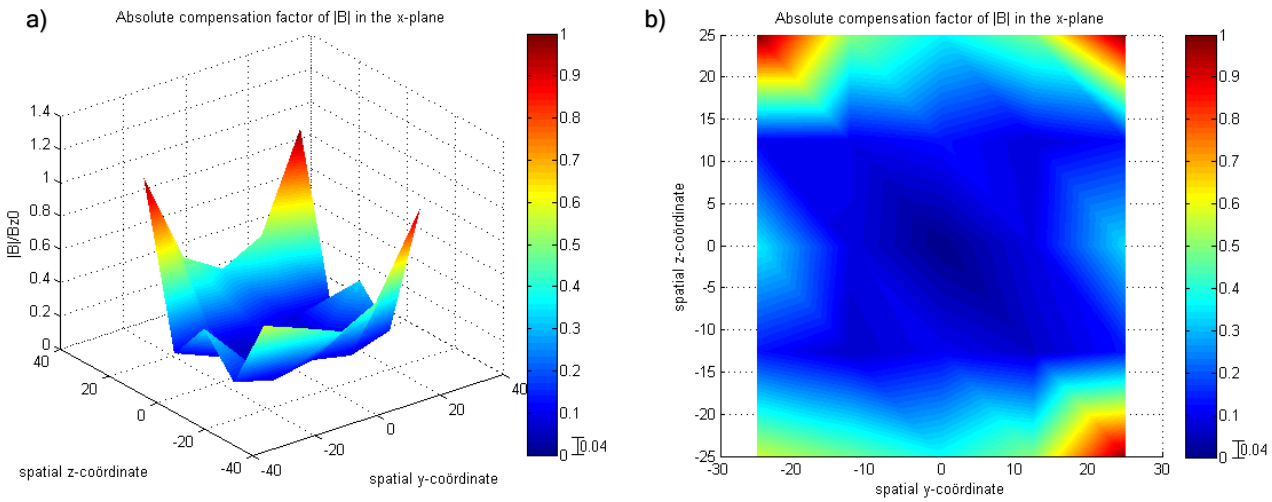

Figure 24: The compensation factor of the total magnetic field |B|, when a strong field is applied in one direction. The axis show the y- and z-coordinates in cm. a) gives a side view, b) the top view.

Compensated field in the region of interest

In this measurement the region of interest is determined for a compensated field. To elaborate on the magnetic field stability of one Helmholtz-like coil set if a large current is applied, a small area is chosen. This area runs from -15 cm to 15 cm in the y- and the z-direction in the x = 0 cm plane, and consists of 49 evenly spread measurement points. To compensate the field the coil constant is used. The components of the field are

$$\boldsymbol{B}_E = \begin{pmatrix} 0.26(2) \\ 0.23(2) \\ 0.39(2) \end{pmatrix} \mathrm{G}$$

at the centre of the Helmholtz cube. To compensate these component wise, a current of -0.59(6)A, -0.52(6)A and -0.88(6)A need to be applied, where the error is determined from both the error in the measured magnetic field and the error for the coil constant. To compensate to a steady level the coils were put under a slightly different current, namely -0.59A, -0.55A and -0.91A for the x, y and z coil respectively. Again the measurement was done using the Gaussmeter.

In figure 25 the results are presented. For a good overview all components are depicted apart, with B_x at the top and B_z at the bottom. A side view and a top view is presented for completeness.

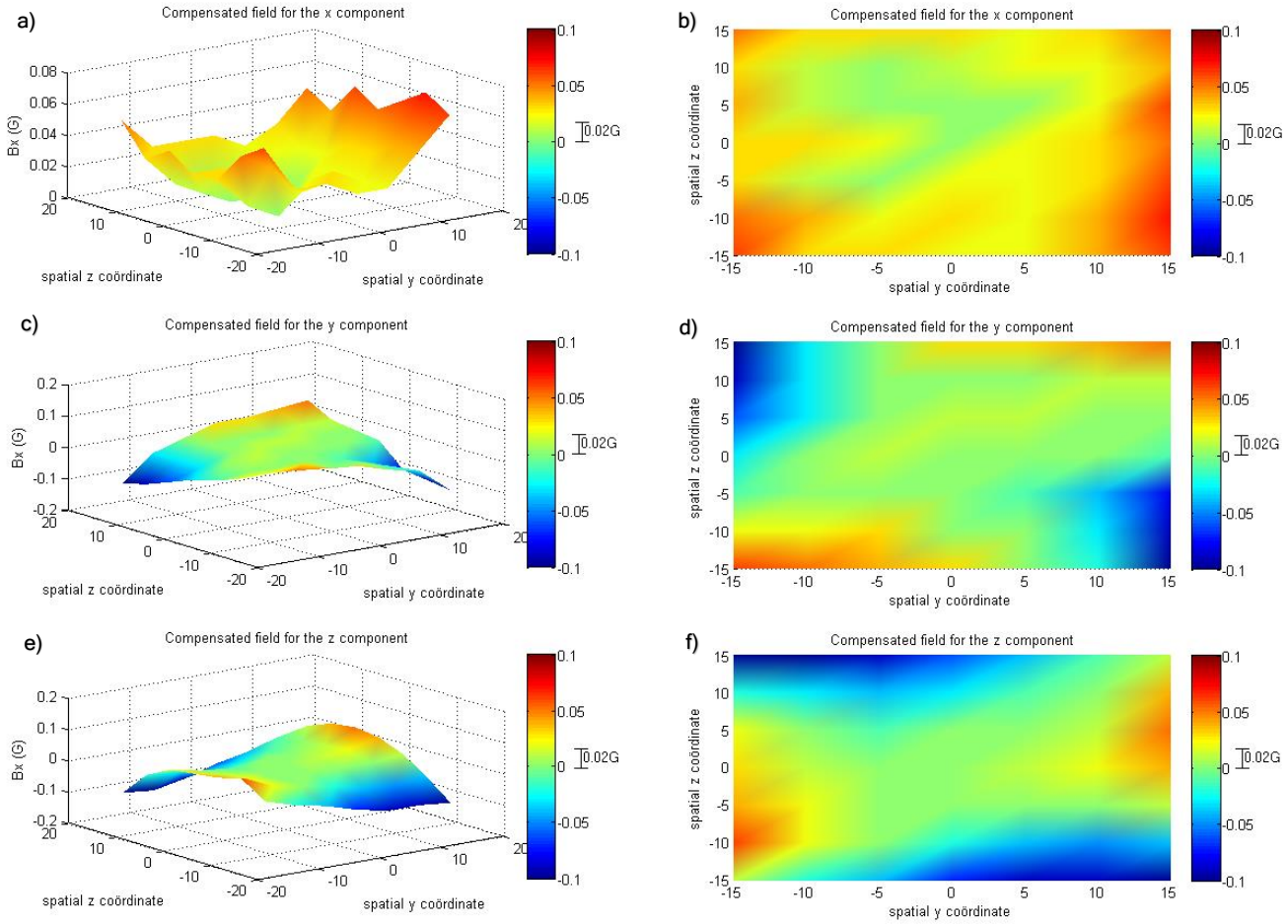

Figure 25: Magnetic field strengths per component given in two sights. The axis show the y- and z-coordinates in cm. Side view: a) Bx c) By e) Bz, top view: b) Bx d) By f) Bz. Note the colour coding for field contours.

For the x-component of the magnetic field a tub-shaped paraboloid is observed. All values of the x-component are positive, and are rising when z and y increase. For the y- and z-component of the magnetic field another structure is observed, the field-components magnitudes have a shape of a saddle, with positive values at the even combinations of the z- and y-directions, while the field goes below zero for the odd combinations. These observations are due to the fact that the points are laying in the x-plane, as can be seen from the one coil set measurement, the shape is primarily caused by the x-coils, but have a slight perturbation from the y-coils. With the same argument the shape of the y- and z-component can be explained. As can be seen from the results of the one coil set experiment (figure 23), the applied field in the z-direction has an effect of on B_y when going outside the central coordinates. The superposition of the two can be well seen from the red stroke south-west and north-east (figure 25d). Having only the y-coils set under current, a picture as 25a would be observed. Yet the z-coils pertubate this image, adding a field as in 25c. Note furthermore that the current on the z-coils exceeds the one on the y-coils. For the z-component the magnitude tends to go negative and is the mirrored version of the y-component. As can be seen, due to the fact that the currents differ, the perturbation of B_z caused by the y-coils is lower. Therefore the measured values in the south-west and north-east corner (figure 25f) are closer to zero, relative to that of the y-component.

Also, in this measurement the total value of the compensated field was measured. This was done with the function on the Gaussmeter, and not by summing over all components. Therefore, the error for these measurement is reduced by a factor $\sqrt{3}$ and remains at the value of 0.02G. The results of this measurement are given in figure 26, where 26a presents a side view and 26b presents a top view. The field magnitude increases the most in the odd corners. This asymmetry is caused by the fact that the currents on the coils are not equal, as the external field had three different components.

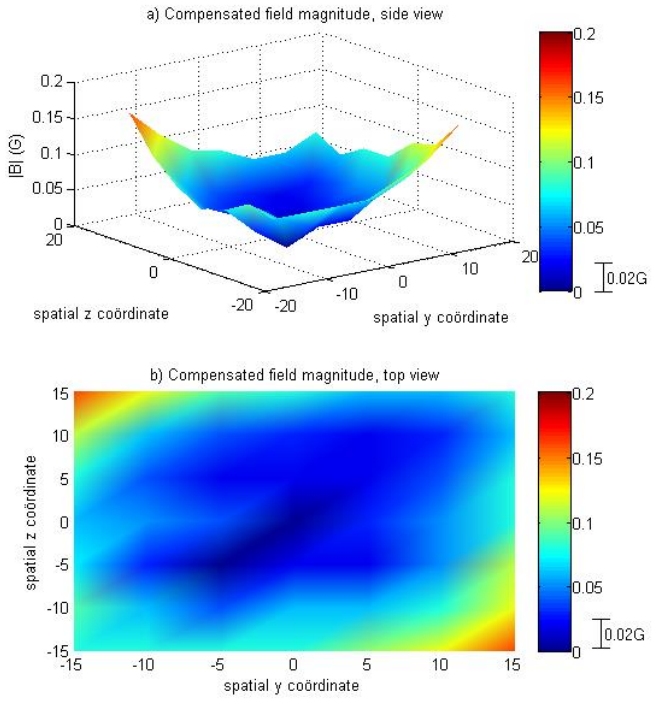

Figure 26: The compensated field magnitude |B|. The axis show the y- and z-coordinates in cm. a) gives a side view, b) the top view.

The compensation factor is defined as the measured compensated field (component) divided by the external field component. Or in mathematical form,

$$c = \frac{|B_{i,r}|}{B_{i,E}},$$

where i = x,y,z or the field magnitude. This describes the compensation relative to the value to be compensated, since the central value is 0.00(2)G for all components. The region of interest is defined as the region where c < 0.1, coming down to e.g. |Bx|<0.026G or |B|<0.05G, for the field magnitude a region where c < 0.05 will also be defined.

In figure 27 the surface plots of the compensation factors per component are given. As can be seen the compensation factors for the y and z component are under 0.05 for a relatively big range. Though, when moving outside this region, the compensation factors go up quickly, leading to a factor above 0.25 at the yellow regions. The compensation factors above 0.25 are only found at the boundaries (y,z = ±15 cm). Yet for our purpose, with the help of extrapolation, coordinates outside a square with a side length of 20 cm will be outside of our region of interest. There should be remarked that the even coordinates show a lower compensation factor. This might be used as

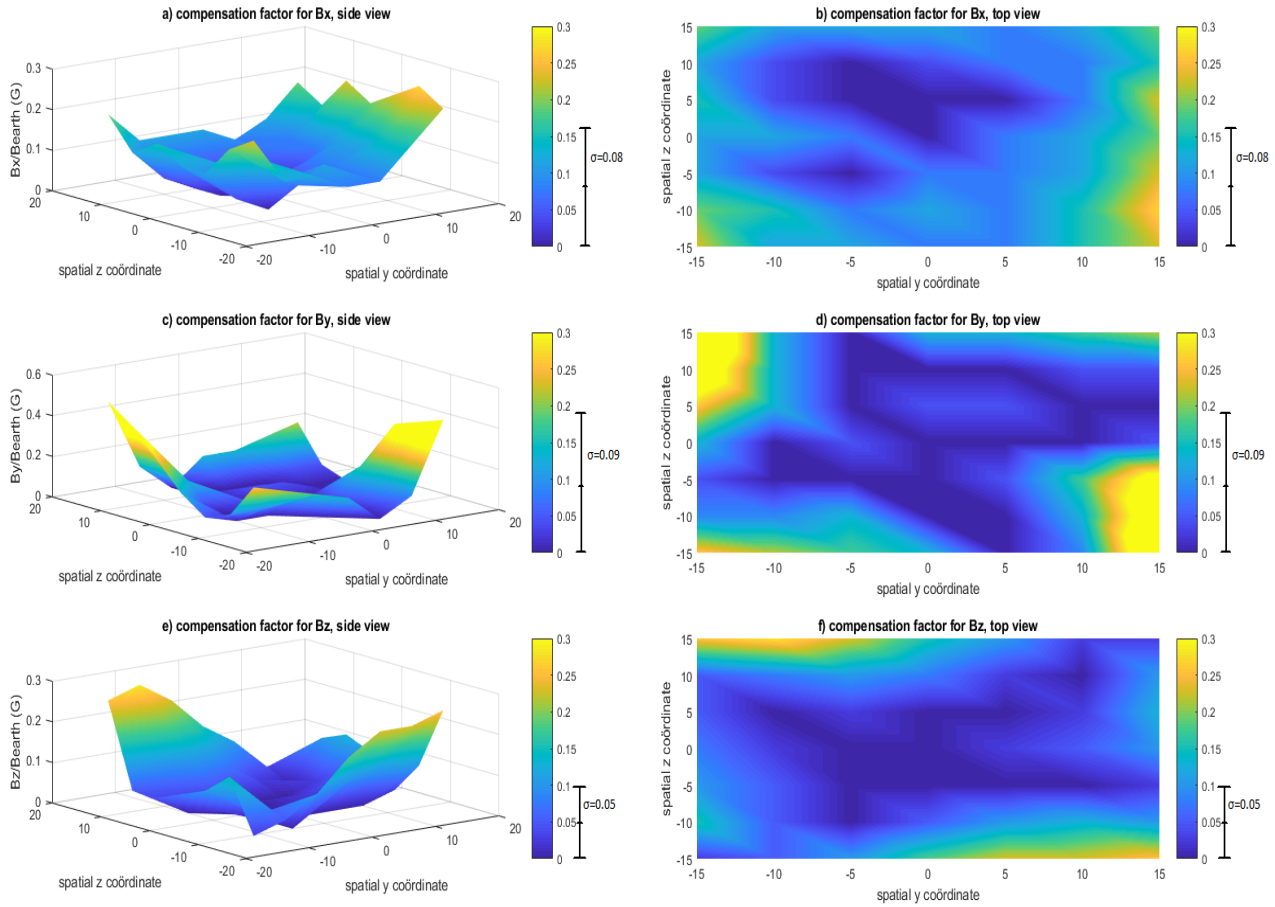

Figure 27: Compensation factors for the magnetic compensated field using a 3 dimensional 62cm Helmholtz-like coil. The axis show the y- and z-coordinates in cm. Side view: a) Bx c) By e) Bz, top view: b) Bx d) By f) Bz.

an advantage for the eEDM search experiment. Moreover we conclude when alike currents are used, the diagonal components will be balanced best.

For the total field the compensation factors are given in figure 28. In figure 28b, two contours are given. The white contour shows the area in which the compensation factor is lower than 0.0577, the mathematical value when |B|=0.03(2)G is divided by B_E=0.52(2)G. And thus gives a region where the total field is less than 0.03(2)G. This region is more spread over the even diagonal coordinates than the odd ones, due to the different currents applied for different directions. The c < 0.1 region is depicted with the black contour, with an addition of a dotted corner, where the compensation factor runs up to 0.15(4) at (y,z) is (10,-10). The asymmetry observed may arise from environmental magnetic asymmetry in the test lab which had not been surveyed on beforehand. Yet (10,-10) is included in the region of interest. Making the region of interest for a 62 cm × 62 cm × 62 cm cubic Helmholtz-like coil configuration 20(3) cm × 20(3) cm × 20(3) cm around the centre, where the error is given by half of the step size between coordinates.

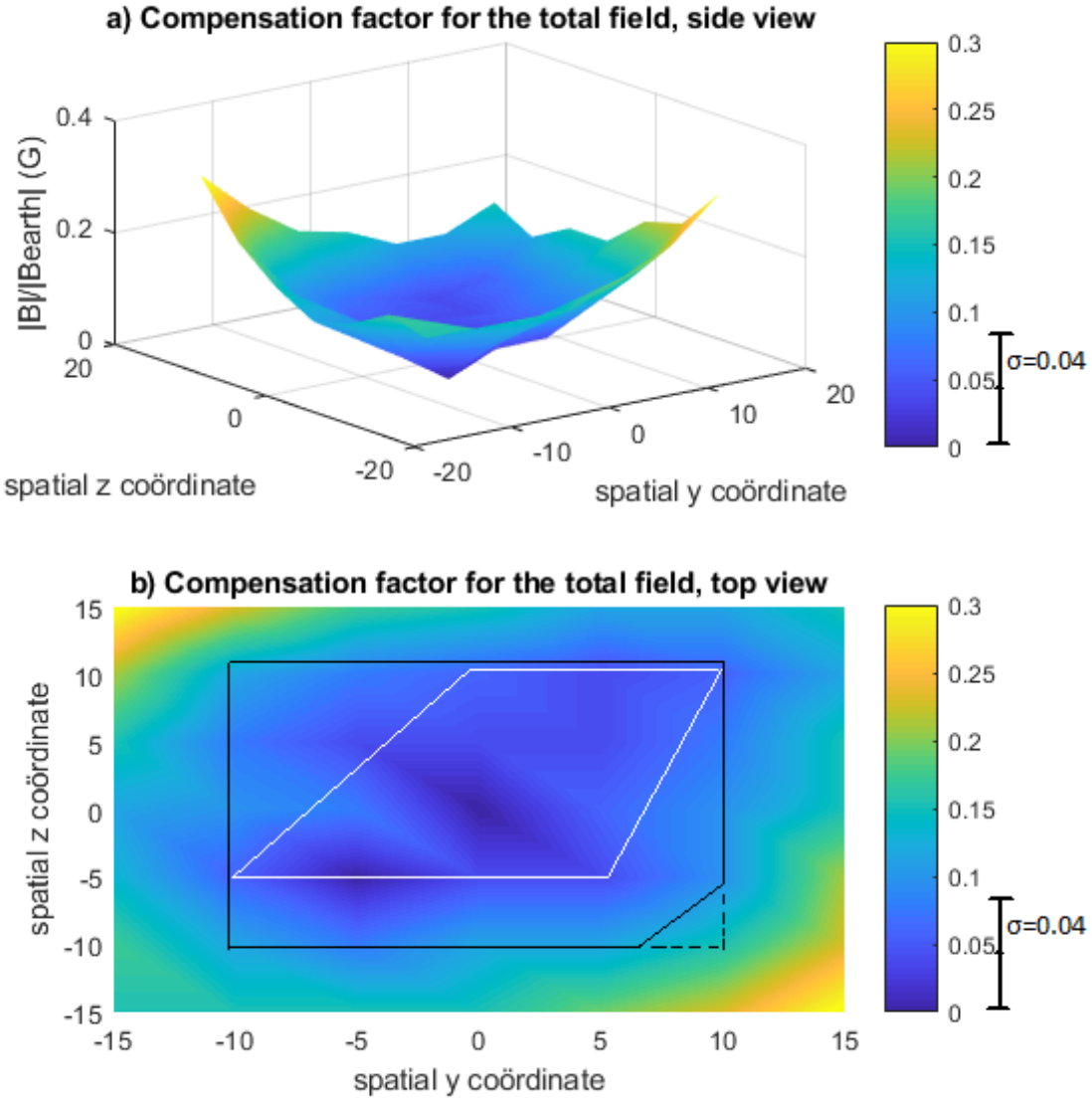

Figure 28: Compensation factor for the total field in the compensated field in a cubic Helmholtz-like configuration of 62 cm length. The axis show the y- and z-coordinates in cm. A side view is given in a), a top view in b). In b) the region where c < 0.1 is contoured black, where c < 0.05 in white.

5. Conclusions and discussion

In the qualitative compensated field measurement it became clear that the cubic Helmholtz-like configuration indeed creates linear fields. Yet, because of this cubic structure the field becomes nonlinear by picking up field components induced by the straight wires for diagonal components. It became clear that a central plane is better compensated than a plane at the boundaries, therefore in subsequent measurements central planes were the scope of the experiments. Via superposition, these measurements could be combined to calculate the field magnitude in different planes.

The coil constant (3.1) has been measured to be 0.44(1) G/A. The coil constant is a linear constant and was equal for all independent directions. This shows the coils are indeed identical.

To investigate the local variation of the external field, a measurement was done without any of the coils set under a current. This measurement showed that the external field was stable inside the configuration, to a limit smaller than the uncertainty of the measurement. The result of these measurement were:

$$\boldsymbol{B}_E = \begin{pmatrix} -0.05(2) \\ 0.38(3) \\ -0.16(2) \end{pmatrix} \text{G}.$$

Where $\boldsymbol{B}_E$ denotes the external magnetic field. Although local stability is proven there are two side notes to these results. Firstly, the room was prepared by removing all magnetic objects at least one meter from the configuration, which might become harder when a larger configuration is used. Secondly, though local stability is proven, there still is a time-dependent variation of the field [33]. As has been seen in other experiment, the external field varied strongly. For the final experiment six weeks later the external field changed to:

$$\boldsymbol{B}_E = \begin{pmatrix} 0.26(2) \\ 0.23(2) \\ 0.39(2) \end{pmatrix} \text{G}.$$

To understand how the field of the Helmholtz-like squared coil, separated by a side length behaves, a measurement with one coil running was conducted. To reduce the relative error from the noise of the Gaussmeter, a strong field was applied. The strength of the induced field was 1.32(3)G with a 3,00(1)A current applied. Two planes were measured, the x-plane and the y-plane, and showed the same result, with B_x and B_y interchanged. The compensation factor, or for this purpose better called stability factor, was defined by 3.2 and assessed per component. For the x-plane, B_x was stable to less than ten per cent for all coordinates. For the y-component a top and bottom value are observed at the coordinates of the wire, making the field stability by less than ten per cent have a '+'-shape. While for the z-component the opposite is observed. The linear field reduces in strength when moving along the y-axis, yet strengthens when moving along the x-axis. When looking at the diagonal coordinates, these effect are superposed and therefore an 'x'-shape arises for the stability factor. For the BaF eEDM search experiment though, the field magnitude is what matters. When analysing the magnetic field strength stability, one sees a stability up to ten percent for a square around the centre with a length of 20 cm.

To define a region of interest a compensated field measurement was executed once again. With an improved set-up and a better guess for the region of interest other coordinates where chosen. Again the field was measured in the x-plane, with both the y- and z-coordinates running from -15 cm to +15 cm.

For the 62 cm × 62 cm × 62 cm Helmholtz-like coil cubic conformation the region of interest is 20(3) cm × 20(3) cm × 20(3) cm. This is proportionately lower than when a circular Helmholtz coil is used, where an area with dimensions R/2 is shielded up to 10%. Yet the use of a true Helmholtz configuration brings some consequences, the coils are twice as large as the distance between them and therefore four times larger than the compensated region. For an area of 1 m, this would yield 4 m. Moreover, construction in three dimensions is harder for circular objects than for squared objects.

There is a clear relationship between the observed field and the combination of the coils. With figure 22 in mind, the coils with the largest current will generate pertubations for the other components. When a cubic structure is used, it is therefore wise to place the cube in such a way that for the external magnetic field, the components are equal. In this way, since the coils are set under equal current, the side effects will cancel out the most and the compensation is more stable with a larger compensated region.

The dimensions of the magnetic compensated region for the BaF eEDM search experiment are 1 m × 0.2 m × 0.2 m. Therefore, to save expenses, it should be examined whether it is necessary to build a symmetric configuration. Though for the y- and z-direction the region in line with their induced fields is just 0.2 m the generated x-component should be stable to 1 m still. Therefore it should be examined if a better stability is obtained for this asymmetric region of interest when rectangular Helmholtz-like coils are used.

Since the region of interest for the BaF is not symmetric, but the x-direction exceeds the other direction by a factor five, it should be examined whether a Maxwell-coil like structure is a better solution. The Maxwell-like coil structure adds a third coil in the centre-plane [39], increasing the stability of the field, and therefore the region of interest. The extra coil makes the induced field more linear, cancelling more off-diagonal components (induced components not in line with the direction of the coil), at first sight this would seem to make the region of interest only wider, yet the length of the region of interest will be larger as well, exactly because of the cancellation of the off-diagonal components. Unfortunately though, a Maxwell-like construction cannot be built for the y- and z-directions, since the centre of these planes lies in the plane of the experiment. A configuration of this kind is given in figure 29, where in blue the circular Maxwell structure is depicted for the compensation in the x-direction, while in green and red rectangular coils for the y- and z-direction is depicted. For the rectangular y- and z-coils, the widths should be larger than 62 cm to have a 20 cm compensated field. To obtain the optimal length further investigation should be done, as for the exact dimensions of the Maxwell configuration.

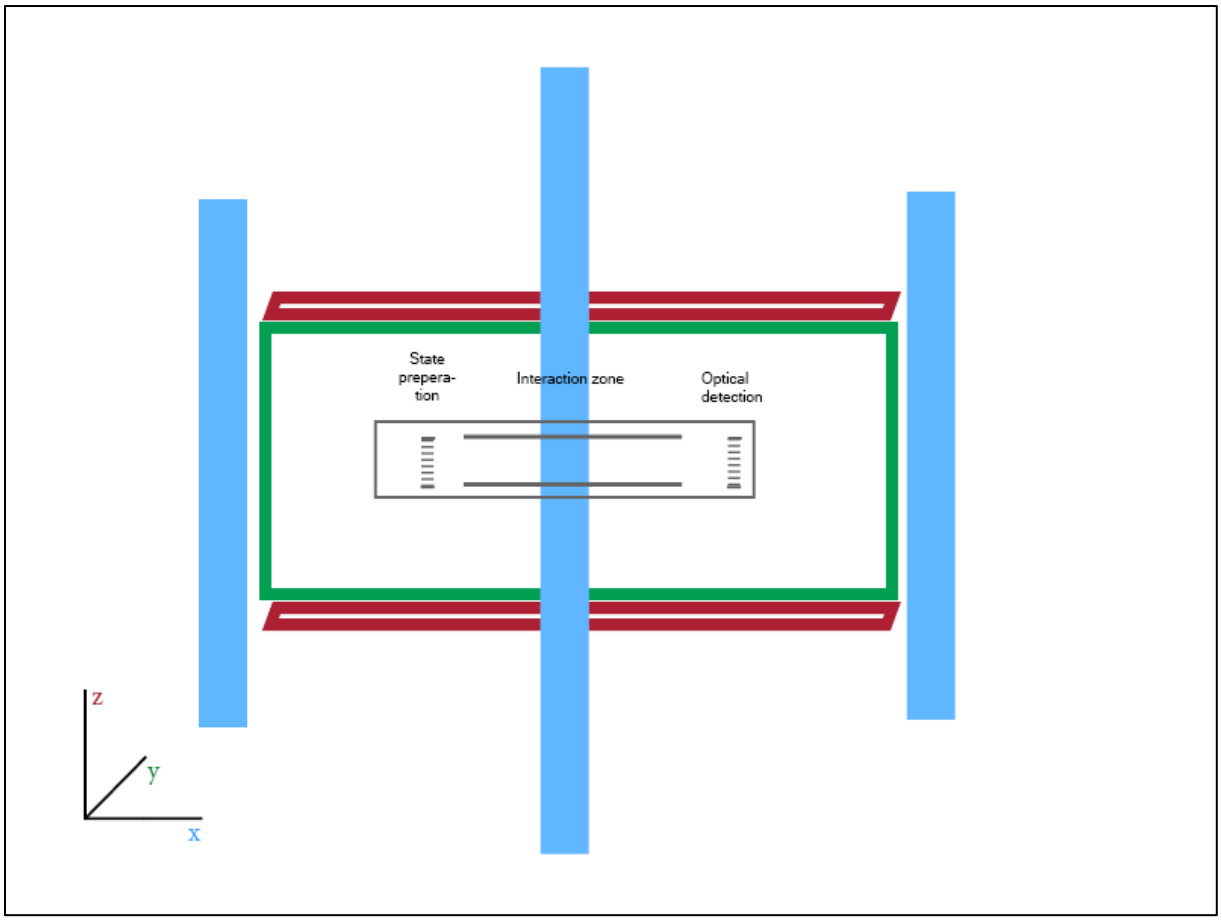

Figure 29: A suggested magnetic compensation system for the BaF eEDM search experiment. In blue Maxwell-like coils focussed on the x-direction, in green rectangular coil for the y direction as in red a rectangular coil for the z direction, in grey the magnetic stable area of the BaF eEDM experiment is depicted.

As mentioned above, the external field is time-dependent. Therefore a feedback loop should be added to the configuration as discussed in section 2.3. Moreover compensation below 10 per cent is by far not enough to obtain $|\mathbf{B}| < 50$ pT. Therefore, about 3 layers of mu-metal should be added. The layers should be positioned as close as possible to the set-up, if not, the outside mu metal layer would pick up the field lines from outside the region of interest. Moreover, as the permeability of metals can drop off when placed in a weak field further investigation should be done regarding using several materials. So will a several mm thick aluminium shield on the outside cancel AC magnetic fields. To generate the homogeneous field needed for the experiment a coil with $\cos(\theta)$ distribution to wire windings can be placed inside the layers of mu metal [40]. With all this in mind, creating a stable magnetic environment that compensates up to 10 per cent, will allow to further decrease the magnetic field to below a level of 50 pT, the level required for the BaF eEDM search experiment.

6. Acknowledgements

Firstly I would like to thank the FIS group of the VSI for this opportunity of doing research in a professional environment. The FIS group has a wide scope of knowledge and it was informative to be a part of this. In particular I would like to thank Klaus Jungmann for his guidance during my research, helping me to straighten my thoughts and being patient whenever I needed the time to understand certain phenomena. Also, I would like to thank Lorentz Willman for inspiring me regarding to particle physics in his lectures.

Also I want to thank my office colleagues Elwin and Alwin for the laughs and helping with the tools to use for my research. I would like to thank Jeroen, with whom I started my bachelor studies, for the mental support during last period. Furthermore I would like to thank Artem for helpful attitude. I also would like to mention Leo Huisman, who besides telling lovely stories about the university back in the days, build parts of the set-up which made my research possible. A special thanks to Thomas, for enthusiastically answering all the questions I had and I'd like to wish him the best of luck in completing the task of creating a compensated field for the BaF experiment.

I would like to thank my family. They provide me unconditional support, with in particular my parents for giving me the flexibility to develop myself to who I am now.

Lastly I would like to thank the University of Groningen for offering me all the tools to successfully apply the knowledge it has given me over time.

7. References

[1] Thomson, J.J. (1897) Cathode Rays. Philosophical Magazine, 44, 293-316. http://dx.doi.org/10.1080/14786449708621070

[2] R. P. Feynman (1949). "Space–Time Approach to Quantum Electrodynamics". Physical Review. 76 (6): 769–89.

[3] R. P. Feynman (1949). "The Theory of Positrons". Physical Review. 76 (6): 749–59.

[4] Fermi, E. (1934). "Versuch einer Theorie der beta-Strahlen. I". Zeitschrift für Physik (in German). 88: 161.

[5] Sheldon L. Glashow, Partial-symmetries of weak interactions, In Nuclear Physics, Volume 22, Issue 4, 1961, Pages 579-588, ISSN 0029-5582, https://doi.org/10.1016/0029-5582(61)90469-2.

[6] E.D. Bloom; et al. (1969). "High-Energy Inelastic e–p Scattering at 6° and 10°". Physical Review Letters. 23 (16): 930–934.

[7] M. Breidenbach; et al. (1969). "Observed Behavior of Highly Inelastic Electron–Proton Scattering". Physical Review Letters. 23 (16): 935–939.

[8] Fritzsch, H.; Gell-Mann, M.; Leutwyler, H. (1973). "Advantages of the color octet gluon picture". Physics Letters. 47B.

[9] T.D. Lee, C.N. Yang, Question of Parity Conservation in Weak Interactions. Phys. Rev. 104 (1956) 254;

[10] C.S. Wu, E. Ambler, R.W. Hayward, D.D. Hoppes, R.P. Hudson, Experimental Test of Parity Conservation in Beta Decay. Phys. Rev. 105 (1957) 1413.

[11] J.H. Christensen, et al., Evidence for the 2π Decay of the K02 Meson. Phys. Rev. Lett. 13 (1964) 138.

[12] Makoto Kobayashi Toshihide Maskawa, CP-Violation in the Renormalizable Theory of Weak Interaction, Progress of Theoretical Physics, Volume 49, Issue 2, 1 February 1973, Pages 652–657

[13] M. Pospelov, A. Ritz, Electric dipole moments as probes of new physics. Annals of Physics 318 (2005) 119–169 165

[14] Becker, Katrin; Becker, Melanie; Schwarz, John (2007). String theory and M-theory: A modern introduction. Cambridge University Press

[15] https://home.cern/about/physics/supersymmetry

[16] The ACME Collaboration, Order of Magnitude Smaller Limit on the Electric Dipole Moment of the Electron, Science 17 Jan 2014: Vol. 343, Issue 6168, pp. 269-272

[17] S. Hoekstra. Physics beyond the standard model with cold molecules: Measuring the electric dipole moment of the electron in BaF. 2016

[18] Griffiths, D. J. Introduction to Electrodynamics, 4th ed., international edition.; Pearson: Boston etc., 2013.

[19] Feynman, R. P.; Leighton, R. B.; Sands, M. L. The Feynman Lectures on Physics; Addison-Wesley: Reading, MA, 1964; Vol. Vol. II, Mainly Electromagnetism and Matter.

[20] N. F. Ramsey, Electric-dipole moments of elementary particles. 1982 Rep. Prog. Phys. 45 95

[21] Lüders, G. "On the Equivalence of Invariance under Time Reversal and under Particle-Antiparticle Conjugation for Relativistic Field Theories" 1954 Kong.Dan.Vid.Sel.Mat.Fys.Med. 28N5 no.5, 1-17

[22] I.B. Khriplovich and S.K. Lamoreaux. CP violation without strangeness – Electric Dipole Moments of particles, Atoms, and Molecules. 1997

[23] CODATA2014, https://physics.nist.gov/cgi-bin/cuu/Value?gf

[24] Nodoka Yamanaka, Analysis of the Electric Dipole Moment in the R-parity Violating Supersymmetric Standard Model, 2013

[25] A C Vutha, W C Campbell, Y V Gurevich, N R Hutzler, M Parsons, D Patterson, E Petrik, B Spaun, J M Doyle, G Gabrielse. Search for the electric dipole moment of the electron with thorium monoxide. 2010. Journal of Physics B: Atomic, Molecular and Optical Physics, Volume 43, Number 7

[26] J. J. Hudson, D. M. Kara, I. J. Smallman, B. E. Sauer, M. R. Tarbutt & E. A. Hinds, Improved measurement of the shape of the electron. Nature 473, 493–496 (26 May 2011)

[27] E.R. Meyer and J.L. Bohn, Prospects for an electron electric-dipole moment search in metastable ThO and ThF^+, Phys. Rev. A 78, 06218 (2006).

[28] M. Abe, G. Gopakumar, M. Hada, B. P. Das, H. Tatewaki, and D. Mukherjee, Application of relativistic coupled-cluster theory to the effective electric field in YbF, Phys. Rev. A 90, 022501 (2014).

[29] L.V. Skripnikov & A.V. Titov, Theoretical study of thorium monoxide for the electron electric dipole moment search: Electronic properties of $H^3\Delta_1$ in ThO, J.Chem. Phys. 142, 024301 (2015).

[30] N. E. Bulleid, S. M. Skoff, R. J. Hendricks, B. E. Sauer, E. A. Hinds, M. R. Tarbutt, Characterization of a cryogenic beam source for atoms and molecules. Phys. Chem. Chem. Phys. 15, 12299 (2013)

[31] Softley Research Group, Stark Decelerator, http://timsoftley.chem.ox.ac.uk/stark-decelerator.aspx

[32] Samuel A. Meek, Maxwell F. Parsons, Georg Heyne, Viktor Platschkowski, Henrik Haak, Gerard Meijer, and Andreas Osterwalder, A traveling wave decelerator for neutral polar molecules, Review of Scientific Instrument 82, 093108 (2011)

[33] T. Burlacu, Magnetic Field Compensation for the BaF eEDM search experiment. Bachelor Thesis. 2017

[34] https://www.ngdc.noaa.gov/geomag-web/#igrfwmm

[35] RAU, M.; COSTANDACHE, D.; BALTAG, O.; IFTEMIE, A.; RAU, I. Dynamic Shielding of the Magnetic Fields. Advances in Electrical and Computer Engineering 2010, 10 (4), 135–142 DOI: 10.4316/aece.2010.04022.

[36] Ramsden, Edward (2006). Hall-effect sensors: theory and applications (2nd ed.).

[37] Jiles, David (1998). Introduction to Magnetism and Magnetic Materials. CRC Press.

[38] http://mumetal.co.uk/?p=106

[39] https://www.alphalabinc.com/content/vector-magnitude-gaussmeter-model-vgm-full/

[40] Clerk-Maxwell, James (1873). *Treatise on Electricity and Magnetism*. **2**. Oxford: The Clarendon Press.

[41] Olivier Grasdijk, PhD thesis, Groningen, 2017 (in prep.)